

1 **Main Text:** Extracellular vesicles (EVs) represent an ancient and conserved form of distant
2 inter-cellular and inter-organismal communication in different physiological and pathological
3 states. EVs carry bioactive cargo to direct development and differentiation, initiate synapse
4 formation in neurons, modulate maturation and fertilization of gametes [1–4]. EVs also may
5 spread toxic cargo, such as unfolded proteins in neurodegenerative diseases or signaling
6 molecules to establish a metastatic niche for cancer cells [5,6]. While EVs are of profound
7 medical importance, the field lacks a basic understanding of how EVs form, what cargo is
8 packaged in different types of EVs originating from same or different cell types, and how
9 different cargoes influence the range of EV targeting and bioactivities.

10 Our study focuses on ciliary EVs that bud from the membrane of cilia, the cellular antennae that
11 receive and transmit signals for intercellular communication. Disrupted ciliary EV signaling is
12 likely an important driver of the pathophysiology of many ciliopathies, such as polycystic kidney
13 disease, retinal degeneration, and others [7]. Ciliary EV biogenesis is an evolutionarily
14 conserved process for which main discoveries were pioneered in the green algae
15 *Chlamydomonas reinhardtii* and free-living nematode *Caenorhabditis elegans* [8,9]. Nematodes
16 use EVs to communicate with mating partners and to modulate and evade host immune
17 responses via specific EV cargo [8,10–15]. Here we used *C. elegans* as a discovery platform to
18 conduct a large-scale isolation and proteomic profiling of environmentally released EVs.

19 **PKD-2, an evolutionarily conserved ciliary EV cargo, enables EV visualization and** 20 **tracking during biochemical enrichment**

21 Our strategy for biochemical EV enrichment relied on the use of a *C. elegans* strain expressing
22 GFP-labeled polycystin-2 (*pkd-2::gfp*), which encodes an evolutionarily conserved cargo of
23 ciliary EVs [8,11]. EVs carrying PKD-2 are shed from the cilia of male-specific sensory neurons
24 (cephalic male CEM and tail ray RnB and hook HOB neurons) into the environment. PKD-2-
25 carrying EVs function in inter-organismal communication by changing male locomotion. Males
26 transfer PKD-2::GFP carrying EVs to vulvae of their mating partners [11,12]. In addition to the
27 PKD-2-expressing sensory neurons, *C. elegans* has a set of sex-shared ciliated neurons whose
28 cilia are exposed and release EVs to the environment – six inner labial type 2 (IL2) neurons
29 (Figure 1A). The male specific PKD-2 expressing neurons and IL2s are collectively termed EV-
30 releasing sensory neurons (EVNs) for their ability to release ciliary EVs with unique and/or
31 common cargo, whereas ciliary EV shedding has not been directly observed from the sex-
32 shared major sensory organs in the head (amphids) and tail (phasmids). Since PKD-2 is a male-
33 specific EV cargo, we used a strain with high incidence of males (*him-5*) and cultured the mixed-
34 sex population on standard bacterial lawns of *E. coli* OP50 favorable for mating to promote the
35 release of signaling ciliary PKD-2 EVs.

36 **Ciliary EV enrichment method**

37 EVs were collected using ultracentrifugation after serial enrichment by several differential
38 centrifugation steps. The resulting crude EV mixture was then resolved using buoyant density
39 centrifugation and high-resolution fractionation (Figure 1B). Collected fractions were profiled to
40 determine their density, protein concentration, and the quantity of PKD-2::GFP EVs using
41 Airyscan confocal imaging (Figure 1C, S1A).

42 In accordance with best practices for EV isolation [16], we tested two protocols of loading EVs
43 for buoyant density centrifugation, top- and bottom-loading for top-down (pelleting) and bottom-
44 up (flotation) gradient equilibration, respectively (Figure 1B). The top-loading method resolved
45 PKD-2::GFP EVs into two sub-populations of 1.11 g/mL (termed “light”) and of 1.14 g/mL
46 (termed “heavy”) densities. The bottom loading resulted in all PKD-2 EVs migrating as a single
47 band that contained both light and heavy PKD-2 EVs (termed “mixed”). Analysis of protein
48 distribution across gradients for both loading approaches showed that 99% of total protein

1 equilibrated at density of 1.18 g/mL and was not associated with the labeled EVs (Figure 1C),
2 indicating that we achieved at least 100-fold enrichment for ciliary PKD-2::GFP EVs.

3 We confirmed the presence of EVs in the fractions-of-interest using transmission electron
4 microscopy (Figure 1D-E). EVs from the PKD-2::GFP-enriched fractions ranged in size from 50
5 nm to 220 nm in diameter (Figure 1F), suggesting heterogeneity of the isolated environmental
6 EVome. In addition to intact EVs, we also observed tubular structures reminiscent of the
7 budding vesicle stems [17] (Figure 1E), indicating that our EV preparations contained
8 membrane-sculpting proteins participating in the formation of EVs.

9 For rigor and reproducibility, we isolated EVs in two more biological replicates using the top-
10 loading method. Each time, PKD-2::GFP-carrying EVs resolved into light and heavy sub-
11 populations. Electrophoresis of proteins isolated from collected EVs revealed greater
12 heterogeneity of the PKD-2 enriched fractions as compared to the fraction with the most protein
13 (1.18 g/ml), where the predominant protein was 35-37 kD (Figure S1B). This size range and
14 density of the band corresponded to bacterial outer membrane proteins (OMPs) [18,19], the
15 major constituents of the outer membrane vesicles (OMVs) released by the *E. coli* culture lawn.
16 OMPs were also present in the PKD-2::GFP enriched fractions, with more prominent presence
17 in the heavy fraction. To increase the depth of protein identification in the subsequent mass
18 spectrometry, we chose not to combine technical replicates (parts of the same biological sample
19 that were run in different density gradient tubes) and treated each as separate samples (Figure
20 S1C-S1E). In addition, we excluded the OMP band prior to mass spectrometry to enrich for the
21 presence of *C. elegans* proteins (Figure S1F). In total, we used 14 samples for protein
22 identification analysis: one mixed fraction from the bottom-loading approach and three top-
23 loaded biological replicates represented by one, two, and three technical replicates, respectively
24 (Figure S1E-S1F).

25 **Protein identification in the fractions enriched with PKD-2::GFP EVs**

26 In total, we obtained 147,132 spectral counts that mapped to the *C. elegans* proteome, with
27 21,254 being unique protein identifiers for 2,888 *C. elegans* proteins and 1,535 peptides that
28 mapped to more than one *C. elegans* protein (Table S1). Pairwise comparison using Spearman
29 correlation analysis showed reproducibility of our approach. Correlation coefficients ranged
30 within 0.72 - 0.88 between technical replicates and 0.43 – 0.76 between biological replicates
31 (Figure S2A) and 60% of the EV cargo candidates were identified in at least 2 out of 3 biological
32 replicates (Figure S2B). Hierarchical clustering analysis segregated all the light fractions from all
33 the heavy ones (Figure S2C), consistent with the idea that the light and heavy EVs might carry
34 unique sets of proteins and/or different amounts of the same proteins. Qualitatively 58% of
35 identified proteins were common between light and heavy fractions, whereas the mixed fraction
36 shared 95% of its proteins with the light and heavy fractions (Figure S2D) consistent with
37 presence of both light and heavy EVs.

38 Light EV fraction was enriched in proteins involved in biosynthesis of amino acids, glycolysis,
39 one-carbon metabolism, nucleocytoplasmic transport, and pentose phosphate pathway, and
40 other carbon metabolic processes (Benjamini-Hochberg adjusted p-value < 0.05). Heavy EV
41 fraction was enriched in gene products involved in oxidative phosphorylation, regulators of ER-
42 associated protein processing and export, glycerophospholipid metabolism, N-glycan
43 biosynthesis, and biosynthesis of unsaturated fatty acids (Benjamini-Hochberg adjusted p-value
44 < 0.05). Overall, the identified EVome was enriched in proteins associated with endocytosis,
45 lysosome, proteasome, phagosome, ribosome, SNARE machinery, TCA cycle, and glutathione
46 metabolism (Figure 2A, Table S2).

47 Of 2,888 identified EV cargo candidates, 2,489 were annotated with InterPro domains.
48 Significant enrichment was established for proteins participating in nucleotide binding, vesicular
49 dynamics, trafficking, glycoproteins, glycoprotein binding proteins, nucleic acid binding, post-

1 translational modifiers, chaperones, redox proteins, proteases, and many proteins with domains
2 known to play a role in protein-protein interactions in signaling cascades (Figure 2B, Table S2).
3 Moreover, specific enrichment was observed in proteins carrying Snf7-like domains, major
4 constituents of the endosomal sorting complex required for transport (ESCRT). Specifically, the
5 Snf7-like domains sculpt membrane bilayers into filaments during vesicle budding [17]. Their
6 enrichment in our EV preparations is consistent with observations of the tubular structures by
7 TEM (Figure 1E). For the full list of the identified ESCRT-associated machinery and its human
8 orthologs see Table S2. Role of the ESCRT machinery in ciliary EV biogenesis is suggested by
9 studies in zebrafish [20,21] and *Chlamydomonas* [22,23], but remains largely unexplored.

10 **Integration with cell-specific transcriptomic datasets**

11 Because the identified EV proteome contained 13% of the entire *C. elegans* proteome, we
12 reasoned that the captured EV cargo candidates likely originated from multiple cellular sources
13 and not solely from the ciliated EV-releasing neurons (EVNs). Nematodes produce EVs from the
14 plasma membrane of embryonic cells [24], epithelial cells and cuticle [25], reproductive tract
15 [26,27], nervous system [11,28,29], and intestine [30]. In these reports, compelling evidence for
16 tissue-specific EV biogenesis was obtained using electron microscopy, whereas EV cargo
17 composition remains unknown.

18 To identify EV cargo originating from the EVNs, we used cell-specific transcriptomic datasets
19 reporting on EVN-enriched transcripts [10,31]. We found 99 gene products (Figure 2C, Table
20 S3) in our EVome that are also enriched in EVNs, including previously identified and confirmed
21 EV cargo such as the polycystins PKD-2 and LOV-1 (a homolog of human PKD1), a
22 myristoylated coiled-coil protein CIL-7 required for environmental EV biogenesis [32], CWP-5 (a
23 protein coexpressed with polycystins), acid-sensing sodium channels ASIC-2 and EGAS-1, and
24 a transmembrane cysteine-rich protein F14D7.11 that belongs to a family of proteins with
25 CYSTM-like domains presumably involved in stress-resistance mechanisms [33]. The presence
26 of these EVN-specific cargo in our EV preparations indicates high degree of enrichment for
27 ciliary EVs given the fact that EVNs occupy less than 0.01% of the whole-body volume [34] and
28 are represented by 27 cells in an adult male and just 6 cells in the hermaphrodite out of almost
29 1000 somatic cells and 2000 germ cells per each animal.

30 Our dataset also contained EVN-specific ciliary proteins that were previously not observed in
31 the process of shedding from cilia. These include a TGF β -like domain-containing protein
32 F28A12.3, an ortholog of human ciliary protein CEP104 - T06D8.2, a tetraspanin-like protein
33 T13F3.7, and mucin-domain containing proteins (F25D7.5, F26C11.3, F59A6.3, and
34 Y70C10A.2). Ciliary kinesin-3 KLP-6, previously known as an EV cargo of mutants lacking EVN-
35 specific tubulin TBA-6 [35], was also found in our EV preparations. Re-evaluation of the KLP-6
36 reporter in the wild-type animals revealed that KLP-6 was shed from the cilia of the IL2 neurons
37 to the environment in the form of ectosomes that bud from ciliary tips (Figure 2D), thereby
38 providing experimental validation for KLP-6 as a member of the EVome. The KLP-6 mammalian
39 homolog KIF13B undergoes EV-release from the ciliary tip in immortalized human retinal
40 pigment epithelial (hTERT-RPE1) cells [36], indicating that cargo of our ciliary EVome are
41 conserved.

42 Comparison to cell-specific transcriptomic datasets captures only proteins that are enriched in
43 the EVNs and depleted from other tissues. Thus, this comparison does not identify cargo
44 produced by both EVNs and larger tissues, such as the intestine or reproductive tract, for
45 vesicular trafficking and EV biogenesis. To overcome this limitation, we developed a relative
46 scoring approach for EV cargo candidates where their expression in a cell-of-interest was
47 compared to their mean expression value in the corresponding group of functionally related cells
48 (e.g., EVNs compared to all neurons taken together). The relative scoring was made possible by
49 single-cell transcriptomic data obtained from profiling hermaphrodites at the 2nd larval stage L2

1 [37]. Due to the lack of such data for *C. elegans* males, we used the sex-shared IL2 EVNs as a
2 proxy for the male-specific EVNs, because of their similarities in transcriptional signatures
3 including expression of components of the ciliary EV biogenesis machinery [10]. The IL2
4 cholinergic neurons were not explicitly identified in the study of Cao *et al* [37], however, all
5 cholinergic neurons of *C. elegans* were segregated into nine types. To determine which of the
6 nine represented the IL2 neurons, we compared their transcriptional signatures to the EVN-
7 specific transcriptome [10] and established that Cholinergic cluster 15 was most related to the
8 EVNs (Figure 2E). We then scored our EV cargoes using two metrics: (x-axis) relative
9 enrichment in the IL2 neurons over mean expression in all neuronal types and (y-axis) relative
10 enrichment in ciliated sensory neurons over mean expression in all tissues (Figure 2F). Scoring
11 EV cargo candidates using these two metrics segregated EV cargo into three categories-of-
12 interest: (i) enriched in IL2 neurons, (ii) enriched in both IL2 and other ciliated neurons, and (iii)
13 enriched in ciliated sensory neurons but excluded from IL2 neurons (Figure 2F). We proceeded
14 with experimental validation of novel EV cargo candidates in all three categories defined by an
15 arbitrary enrichment ratio of more than 5-fold (Figure S3A).

16 **Cilia produce EVs that carry nucleic acid-binding proteins SID-2, ENPP-1, and MCM-3**

17 SID-2 (systemic RNA interference defective) is a double stranded RNA (dsRNA) transporter
18 required for environmental RNAi in *C. elegans*. SID-2 internalizes ingested dsRNA from the
19 intestinal lumen, the first step in the systemic silencing of gene expression [38–40]. The native
20 function of SID-2 remains unknown. Intrigued by this and the abundance of SID-2 in our EV
21 preparations, we examined SID-2 endogenous expression and protein localization patterns
22 using C-terminal mScarlet fluorescent tag, engineered by CRISPR/Cas9-mediated insertion into
23 the *sid-2*-coding region in the genome (Figure S3B). The resulting SID-2::mScarlet reporter was
24 co-expressed with PKD-2::GFP in male-specific EVNs, as well as in intestine and excretory
25 system in both males and hermaphrodites (Figure 3A, S3D-E). SID-2::mScarlet was abundant
26 on the apical surface of the intestine, consistent with its known role in endocytosis of dsRNA
27 (Figure S3C) [38–40].

28 In male-specific EVNs, SID-2::mScarlet was abundant at the ciliary base regions, suggesting
29 that its primary function in these neurons is associated with the cilia. We also observed SID-
30 2::mScarlet being environmentally released in the form of ciliary EVs (Figure 3B-C). Because
31 SID-2 is a transmembrane RNA-binding protein, its presence in ciliary EVs suggests that ciliary
32 EVs might be capable of transporting RNA. To our knowledge this is the first report of an RNA-
33 binding protein as a cargo of ciliary EVs, suggesting that *C. elegans* cilia possess molecular
34 machinery for extracellular transport of RNA.

35 ENPP-1 (C27A7.1), an ortholog of human ectonucleotide pyrophosphatase phosphodiesterases
36 (ENPPs), is another nucleic acid binding candidate cargo that co-segregated with known EVN-
37 specific EV cargo (Figure 2F). ENPPs are esterases that hydrolyze phosphodiester linkages in
38 either nucleotides (e.g. ENPP1) or lysophospholipids (e.g. ENPP2, aka Autotaxin) [41].
39 Comparative analysis of C27A7.1 to mammalian ENPP-1 and ENPP-2 showed that C27A7.1
40 possesses sequence determinants of substrate preference for nucleotides, and not for
41 lysophospholipids [42] (Figure S4A). Hence, we referred to C27A7.1 as ENPP-1 and generated
42 an ENPP-1::mScarlet transgenic translational reporter.

43 ENPP-1::mScarlet showed a speckled presence in the EVNs, with specific accumulations in the
44 cilia of the CEM and shared IL2 neurons in the head and ray RnB neurons in the male tail
45 (Figure 4A-B, S4B-D). The ENPP-1::mScarlet was released in environmental EVs from both
46 CEMs and IL2s (Figure 4A-B, Movie S1). ENPP-1::mScarlet EV shedding from IL2s was
47 qualitatively different from CEM EV shedding: the tips of IL2 cilia occasionally shed large ENPP-
48 1 and KLP-6 carrying EVs via ectocytosis (Figure 2D), whereas CEMs abundantly shed smaller
49 EVs. Taken together our data establish the cilium as a cellular location for ENPP-1 EV

1 shedding. Consistent with a role in cilia, mammalian ENPP1 loss-of-function manifests signs of
2 ciliopathies, such as accelerated ossification, hearing impairment, altered insulin metabolism
3 and immune response [43–46].

4 To validate the IL2-enriched category of EV cargo candidates (Category I, Figure 2F), we
5 focused on another nucleic acid binding protein, MCM-3 (minichromosome maintenance
6 complex component 3 licensing factor) and generated transgenic animals expressing MCM-
7 3::mScarlet driven by its native promoter. Strikingly, MCM-3::mScarlet was specifically enriched
8 in the cytoplasm of all EVNs in adult animals and in their cilia and co-localized with PKD-2::GFP
9 (Figure 5A, S5A-B). MCM-3::mScarlet was released from the cilia in the form of EVs. MCM-
10 3::mScarlet was also expressed in the developing embryo where it showed nuclear localization
11 consistent with the known function of the MCM proteins in DNA replication licensing and DNA
12 helicase activity of the MCM-2-7 complex [47] (Figure S5C).

13 Functions of MCM proteins outside of replication are known within Metazoa. For example, a
14 paralog of MCM-3, the MCM2 protein, is required for normal cilia function during *Zebrafish*
15 development [48] and is enriched in sensory ciliated hair cells of the inner ear [49]. Mutations in
16 human *MCM2* are associated with autosomal dominant deafness. Our finding that *mcm-3* is
17 expressed in sensory ciliated EVNs of *C. elegans* suggests a conserved role for MCM
18 components in the physiology of ciliated cells and ciliary EV signaling.

19 Finally, we also explored EV cargo candidates enriched in the ciliated neurons but specifically
20 excluded from IL2 neurons (Category III, Figure 2F). For that, we examined the expression
21 pattern of TSP-6, an ortholog of human tetraspanin CD9, a marker for human extracellular
22 vesicle isolation [16] (Figure 5B-C). The TSP-6::mScarlet was present in filament-like branches
23 of the chemosensory AWA cilium, rod-like amphid channel cilia of the head, as well as the
24 phasmid cilia of the tail (Figure S5D-E) but was not visibly expressed in EVNs. We observed the
25 TSP-6-carrying EVs being released from a channel of the amphid sensillum (Figure 5C). At the
26 time of this writing TSP-6 was independently discovered as an EV cargo that can also be taken
27 by surrounding amphid glial cell [50], suggesting the role of EVs in the neuron-glia crosstalk.
28 Collectively, these findings open a new field of studying ciliary EVs in diverse ciliary contexts in
29 *C. elegans* and suggests that all cilia may have the potential to shed EVs.

30 **Males transfer seminal EVs to the hermaphrodite uterus during mating**

31 We also observed that ENPP-1::mScarlet localized to the male reproductive tract. The ENPP-
32 1::mScarlet localization pattern in the secretory cuboidal cells of the vas deferens resembled
33 giant multivesicular bodies (MVB) forming intrusions reminiscent of an ongoing exosome-
34 formation process (Figure 6A, S4D). ENPP-1 localization to the male reproductive tract is
35 consistent with reports of ENPP3 being abundant in the EVs of the epididymal fluid of mammals
36 [51,52]. Thus, we tested whether the ENPP-1 EVs were transferred from males to
37 hermaphrodite partners during mating. We paired an *enpp-1::mScarlet*-expressing male to a
38 non-fluorescent hermaphrodite for copulation (Figure 6B) and observed ENPP-1::mScarlet EV
39 release from the male tail as he backed along the hermaphrodite's body scanning for the vulva
40 (Movie S2). Upon inserting his copulatory spicules through the vulva, the male transferred
41 seminal fluid containing ENPP-1::mScarlet EVs into the uterus (Figure 6C, Movie S2). We
42 hypothesize that the giant MVB-like structures of the *C. elegans* reproductive tract are an
43 equivalent of the apocrine secretions of the epididymal epithelium of mammals that carry loads
44 of smaller EVs into the seminal fluid [2], ENPP-1 EVs maybe similar to mammalian
45 epididymosomes that are of densities similar to PKD-2::GFP EVs [53]. Overall, these
46 observations indicate that the same EV cargo can function in multiple tissues with different
47 modes of EV biogenesis, i.e. ectocytosed in the form of ciliary EVs or released from MVBs as
48 exosomes.

1 Since our dataset contained seminal fluid EVs, we proceeded to compare our dataset with the
2 list of gene products overrepresented in males as identified by bulk transcriptomics [54] (Figure
3 5D, Table S3). We found 244 male-enriched or male-specific gene products, among which more
4 than 50% were predicted to originate from the male reproductive tract, whereas others were
5 predicted to arise from male-specific neurons or glia (Figure 5E). Thus, our study represents the
6 first report of a male-specific EV proteome that largely expands the list of conserved and
7 species-specific animal EV cargo.

8 **Data mining tool to identify cell- and tissue- specific EVomes**

9 Our dataset can be mined to predict tissue-specific EV cargo shed into the environment using
10 the same scoring approach we used to identify new ciliary EV cargo. For example, among
11 hypodermis-specific peptides (Figure S6A), we found proteins involved in maintenance of cuticle
12 integrity. Those include CPI-1 inhibitor of cysteine proteinases, which are often used by plants
13 as nematocidal agents [55], and NIT-1 nitrilase, a hydrolase of deaminated glutathione [56], that
14 is a likely byproduct of glutathione-mediated cuticular shedding during molting [57]. We also
15 found GRD-3, a hedgehog-related protein specific to seam cells. Seam cells are known to
16 release exosomes to build alae [58], cuticular ridges running along the *C. elegans* body. Other
17 hypodermis-enriched EV cargo candidates included proteins involved in cholesterol and one-
18 carbon metabolism (SAMS-1, SAMT-1, PMT-1, PMT-2) [59,60], and melanin/tyrosine
19 metabolism (PAH-1, HPD-1, TYR-4) [61–64]. Cuticle composition is regulated in response to
20 different developmental and environmental cues [65–67]. We hypothesize that one way to
21 achieve this would be to deliver matrix-modifying enzymes in the form of EVs to the cuticular
22 extracellular space.

23 Another example of an EV source tissue that was highly represented in our EVome was the
24 germline (Figure S6B). The germline-specific EV cargo candidates included proteins implicated
25 in formation of extracellular matrix of the eggshell (EGG-1, EGG-2, EGG-6, PERM-4, CBD-1,
26 CPG-1, CPG-2, GLD-1) [65] and RNA metabolism associated with germ granules: Y-box
27 binding proteins, orthologs of YBX1 implicated in sorting RNAs into EVs (CEY-1, CEY-2, CEY-3,
28 CEY-4) [68,69], Argonautes (CSR-1, PPW-1, PPW-2, WAGO-1, WAGO-4) [70], P-granule
29 assembly proteins (CGH-1, PGL-1, PGL-3, DEPS-1, EGO-1, PID-2, PRG-1, ELLI-1, GLH-1,
30 OMA-1, PUF-5) [71], and many other nucleic acid binding proteins, such as RUVB-1, M28.5, all
31 MCM family members (for the full list refer to Table S2). Overall, overrepresentation of nucleic
32 acid binding proteins (Figure 2B, Table S2) in our dataset suggests that environmental EVs
33 could serve as vectors for horizontal transfer of genetic information and regulation of gene
34 expression in trans.

35 **Discussion**

36 Our work establishes *C. elegans* as a discovery platform for animal EV biology. We obtained a
37 much greater depth of *C. elegans* EV protein identification than in previous studies [72,73] via
38 use of a mixed-stage *C. elegans* population with males and hermaphrodites, enrichment via
39 buoyant density centrifugations, and direct visualization of GFP-labeled EV fractions of interest.
40 The proteogenomic mining approach that we applied to EV cargo candidates lead to the
41 discovery of four novel ciliary EV cargoes. Based on *in vivo* fluorescent protein-tagging and
42 imaging, none of the newly discovered cargoes co-localized to PKD-2 on ciliary EVs, indicating
43 great complexity and heterogeneity of the EV mixture that co-purifies with PKD-2 EVs. Our
44 results show that EVs shed by different neuronal types carry distinct EV cargo and corroborate
45 our previous report that a single neuronal cilium may shed multiple cargoes [13].

46 Enrichment of our dataset in nucleic acid binding proteins is in agreement with findings of
47 abundant small RNAs carried by EVs of parasitic nematodes [14]. Our work demonstrates that
48 ciliary EVs carry RNA- and DNA- binding proteins, suggesting that cilia may play a role in
49 horizontal transfer of genetic information. Many EV cargo candidates were predicted to originate

1 from the male reproductive tract and thus might play roles in regulation of gene expression [74],
2 fitness of male spermatozoa, male fertility, and sexual interactions [75].

3 *C. elegans* offers many advantages as a discovery system for identifying EV cargo,
4 mechanisms of EV biogenesis, and EV-based communication pathways, including genetic
5 tractability, *in vivo* imaging and bioassays, and scalability necessary for identification of rare
6 and/or signaling-induced EV cargoes. Our proteogenomic mining strategy can be applied to any
7 cell- or tissue-of-interest using the MyEVome Web App. We envision that our dataset can be
8 exploited and used as an experimental springboard in three different ways: (i) identification of
9 conserved and species-specific drivers of EV-based communication in general, and ciliary EV
10 biogenesis in particular, (ii) discovery of novel bioactivities that have not been associated with
11 extracellular vesicles, (iii) in combination with other identified EV proteomes, understanding of
12 evolutionary specialization of EV-based communication within Nematoda clades, including
13 parasites that affect up to a quarter of the human population [76].

14 **References and Notes**

- 15 1. Sung, B.H., Parent, C.A., and Weaver, A.M. (2021). Extracellular vesicles: Critical players
16 during cell migration. *Dev. Cell*. Available at: <https://doi.org/10.1016/j.devcel.2021.03.020>.
- 17 2. Foot, N.J., and Kumar, S. (2021). The Role of Extracellular Vesicles in Sperm Function
18 and Male Fertility. In *Subcellular Biochemistry*, pp. 483–500.
- 19 3. Jiang, X., You, L., Zhang, Z., Cui, X., Zhong, H., Sun, X., Ji, C., and Chi, X. (2021).
20 Biological Properties of Milk-Derived Extracellular Vesicles and Their Physiological
21 Functions in Infant. *Front. Cell Dev. Biol.* 9, 1–13.
- 22 4. Lizarraga-Valderrama, L.R., and Sheridan, G.K. (2021). Extracellular vesicles and
23 intercellular communication in the central nervous system. *FEBS Lett.* 595, 1391–1410.
- 24 5. Urabe, F., Patil, K., Ramm, G.A., Ochiya, T., and Soekmadji, C. (2021). Extracellular
25 vesicles in the development of organ-specific metastasis. *J. Extracell. Vesicles* 10, 6097.
26 Available at: <https://www.mdpi.com/1422-0067/21/17/6097>.
- 27 6. Aires, I.D., Ribeiro-Rodrigues, T., Boia, R., Ferreira-Rodrigues, M., Girão, H., Ambrósio,
28 A.F., and Santiago, A.R. (2021). Microglial extracellular vesicles as vehicles for
29 neurodegeneration spreading. *Biomolecules* 11, 1–23.
- 30 7. Ding, H., Li, L.X., Harris, P.C., Yang, J., and Li, X. (2021). Extracellular vesicles and
31 exosomes generated from cystic renal epithelial cells promote cyst growth in autosomal
32 dominant polycystic kidney disease. *Nat. Commun.* 12, 1–18. Available at:
33 <http://dx.doi.org/10.1038/s41467-021-24799-x>.
- 34 8. Wang, J., and Barr, M.M. (2018). Cell–cell communication via ciliary extracellular
35 vesicles: clues from model systems. *Essays Biochem.* 62, 205–213.
- 36 9. Wood, C.R., and Rosenbaum, J.L. (2015). Ciliary ectosomes: Transmissions from the
37 cell’s antenna. *Trends Cell Biol.* 25, 276–285. Available at:
38 <http://dx.doi.org/10.1016/j.tcb.2014.12.008>.
- 39 10. Wang, J., Kaletsky, R., Silva, M., Williams, A., Haas, L.A., Androwski, R.J., Landis, J.N.,
40 Patrick, C., Rashid, A., Santiago-Martinez, D., *et al.* (2015). Cell-Specific Transcriptional
41 Profiling of Ciliated Sensory Neurons Reveals Regulators of Behavior and Extracellular
42 Vesicle Biogenesis. *Curr. Biol.* 25, 3232–3238.
- 43 11. Wang, J., Silva, M., Haas, L.A., Morsci, N.S., Nguyen, K.C.Q., Hall, D.H., and Barr, M.M.
44 (2014). *C. elegans* ciliated sensory neurons release extracellular vesicles that function in
45 animal communication. *Curr. Biol.* 24, 519–525.

- 1 12. Wang, J., Nikonorova, I.A., Gu, A., Sternberg, P.W., and Barr, M.M. (2020). Release and
2 targeting of polycystin-2-carrying ciliary extracellular vesicles. *Curr. Biol.* *30*, R755–R756.
- 3 13. Wang, J., Nikonorova, I., Silva, M., Walsh, J., Tilton, P., Gu, A., Akella, J., and Barr, M.M.
4 (2021). Sensory Cilia Act as a Specialized Venue for Regulated Extracellular Vesicle
5 Biogenesis and Signaling. *SSRN Electron. J.*, 1–9. Available at:
6 <https://doi.org/10.1016/j.cub.2021.06.040>.
- 7 14. Cai, Q., He, B., Weiberg, A., Buck, A.H., and Jin, H. (2019). Small RNAs and extracellular
8 vesicles: New mechanisms of cross-species communication and innovative tools for
9 disease control. *PLoS Pathog.* *15*, 1–13. Available at:
10 <http://dx.doi.org/10.1371/journal.ppat.1008090>.
- 11 15. Drurey, C., and Maizels, R.M. (2021). Helminth extracellular vesicles: Interactions with
12 the host immune system. *Mol. Immunol.* *137*, 124–133. Available at:
13 <https://doi.org/10.1016/j.molimm.2021.06.017>.
- 14 16. Théry, C., Witwer, K.W., Aikawa, E., Alcaraz, M.J., Anderson, J.D., Andriantsitohaina, R.,
15 Antoniou, A., Arab, T., Archer, F., Atkin-Smith, G.K., *et al.* (2018). Minimal information for
16 studies of extracellular vesicles 2018 (MISEV2018): a position statement of the
17 International Society for Extracellular Vesicles and update of the MISEV2014 guidelines.
18 *J. Extracell. Vesicles* *7*.
- 19 17. Tang, S., Henne, W.M., Borbat, P.P., Buchkovich, N.J., Freed, J.H., Mao, Y., Fromme,
20 J.C., and Emr, S.D. (2015). Structural basis for activation, assembly and membrane
21 binding of ESCRT-III Snf7 filaments. *Elife* *4*, 1–22.
- 22 18. Lee, E.Y., Joo, Y.B., Gun, W.P., Choi, D.S., Ji, S.K., Kim, H.J., Park, K.S., Lee, J.O., Kim,
23 Y.K., Kwon, K.H., *et al.* (2007). Global proteomic profiling of native outer membrane
24 vesicles derived from *Escherichia coli*. *Proteomics* *7*, 3143–3153.
- 25 19. Chutkan, H., MacDonald, I., Manning, A., and Kuehn, M.J. (2013). Quantitative and
26 Qualitative Preparations of Bacterial Outer Membrane Vesicles. In *Methods in Molecular*
27 *Biology*, pp. 259–272.
- 28 20. Jung, E., Choi, T.I., Lee, J.E., Kim, C.H., and Kim, J. (2020). ESCRT subunit CHMP4B
29 localizes to primary cilia and is required for the structural integrity of the ciliary
30 membrane. *FASEB J.* *34*, 1331–1344.
- 31 21. Ott, C., Nachmias, D., Adar, S., Jarnik, M., Sherman, S., Birnbaum, R.Y., Lippincott-
32 Schwartz, J., and Elia, N. (2018). VPS4 is a dynamic component of the centrosome that
33 regulates centrosome localization of γ -tubulin, centriolar satellite stability and ciliogenesis.
34 *Sci. Rep.* *8*, 1–19.
- 35 22. Diener, D.R., Lupetti, P., and Rosenbaum, J.L. (2015). Proteomic analysis of isolated
36 ciliary transition zones reveals the presence of ESCRT proteins. *Curr. Biol.* *25*, 379–384.
37 Available at: <http://dx.doi.org/10.1016/j.cub.2014.11.066>.
- 38 23. Long, H., Zhang, F., Xu, N., Liu, G., Diener, D.R., Rosenbaum, J.L., and Huang, K.
39 (2016). Comparative Analysis of Ciliary Membranes and Ectosomes. *Curr. Biol.* *26*,
40 3327–3335. Available at: <http://dx.doi.org/10.1016/j.cub.2016.09.055>.
- 41 24. Beer, K.B., Rivas-Castillo, J., Kuhn, K., Fazeli, G., Karmann, B., Nance, J.F., Stigloher,
42 C., and Wehman, A.M. (2018). Extracellular vesicle budding is inhibited by redundant
43 regulators of TAT-5 flippase localization and phospholipid asymmetry. *Proc. Natl. Acad.*
44 *Sci. U. S. A.* *115*, E1127–E1136.
- 45 25. Liégeois, S., Benedetto, A., Michaux, G., Belliard, G., and Labouesse, M. (2007). Genes
46 required for osmoregulation and apical secretion in *Caenorhabditis elegans*. *Genetics*

- 1 175, 709–724.
- 2 26. Kosinki, M., McDonald, K., Schwartz, J., Yamamoto, I., and Greenstein, D. (2005). *C.*
3 *elegans* sperm bud vesicles to deliver a meiotic maturation signal to distant oocytes.
4 *Development* 132, 3357–3369.
- 5 27. Cohen, J.D., Sparacio, A.P., Belfi, A.C., Forman-Rubinsky, R., Hall, D.H., Maul-Newby,
6 H., Frand, A.R., and Sundaram, M. V. (2020). A multi-layered and dynamic apical
7 extracellular matrix shapes the vulva lumen in *Caenorhabditis elegans*. *Elife* 9, 1–77.
8 Available at: <https://elifesciences.org/articles/57874>.
- 9 28. Melentijevic, I., Toth, M.L., Arnold, M.L., Guasp, R.J., Harinath, G., Nguyen, K.C., Taub,
10 D., Parker, J.A., Neri, C., Gabel, C. V., *et al.* (2017). *C. elegans* neurons jettison protein
11 aggregates and mitochondria under neurotoxic stress. *Nature* 542, 367–371.
- 12 29. Oren-Suissa, M., Gattegno, T., Kravtsov, V., and Podbilewicz, B. (2017). Extrinsic repair
13 of injured dendrites as a paradigm for regeneration by fusion in *Caenorhabditis elegans*.
14 *Genetics* 206, 215–230.
- 15 30. Buck, A.H., Coakley, G., Simbari, F., McSorley, H.J., Quintana, J.F., Le Bihan, T., Kumar,
16 S., Abreu-Goodger, C., Lear, M., Marcus, Y., *et al.* (2014). Exosomes secreted by
17 nematode parasites transfer small RNAs to mammalian cells and modulate innate
18 immunity. *Nat. Commun.* 5.
- 19 31. Ebbing, A., Vértessy, Á., Betist, M.C., Spanjaard, B., Junker, J.P., Berezikov, E., van
20 Oudenaarden, A., and Korswagen, H.C. (2018). Spatial Transcriptomics of *C. elegans*
21 Males and Hermaphrodites Identifies Sex-Specific Differences in Gene Expression
22 Patterns. *Dev. Cell* 47, 801-813.e6.
- 23 32. Maguire, J.E., Silva, M., Nguyen, K.C.Q., Hellen, E., Kern, A.D., Hall, D.H., and Barr,
24 M.M. (2015). Myristoylated CIL-7 regulates ciliary extracellular vesicle biogenesis. *Mol.*
25 *Biol. Cell* 26, 2823–2832.
- 26 33. Venancio, T.M., and Aravind, L. (2010). CYSTM, a novel cysteine-rich transmembrane
27 module with a role in stress tolerance across eukaryotes. *Bioinformatics* 26, 149–152.
- 28 34. Froehlich, J.J., Rajewsky, N., and Ewald, C.Y. (2021). Estimation of *C. elegans* cell- and
29 tissue volumes. *microPublication Biol.* 2021, 2–5. Available at:
30 <http://www.ncbi.nlm.nih.gov/pubmed/33426507>
31 <http://www.pubmedcentral.nih.gov/articlerender.fcgi?artid=PMC7783529>.
- 32 35. Silva, M., Morsci, N., Nguyen, K.C.Q., Rizvi, A., Rongo, C., Hall, D.H., and Barr, M.M.
33 (2017). Cell-Specific α -Tubulin Isozyme Regulates Ciliary Microtubule Ultrastructure,
34 Intraflagellar Transport, and Extracellular Vesicle Biology. *Curr. Biol.* 27, 968–980.
- 35 36. Juhl, A.D., Anvarian, Z., Berges, J., Wüstner, D., and Lotte, B. (2021). Transient
36 accumulation and bidirectional movement of KIF13B in primary cilia.
- 37 37. Cao, J., Packer, J.S., Ramani, V., Cusanovich, D.A., Huynh, C., Daza, R., Qiu, X., Lee,
38 C., Furlan, S.N., Steemers, F.J., *et al.* (2017). Comprehensive single-cell transcriptional
39 profiling of a multicellular organism. *Science* (80-.). 357, 661–667. Available at:
40 <https://www.sciencemag.org/lookup/doi/10.1126/science.aam8940>.
- 41 38. McEwan, D.L., Weisman, A.S., and Hunter, C.P. (2012). Uptake of Extracellular Double-
42 Stranded RNA by SID-2. *Mol. Cell* 47, 746–754. Available at:
43 <http://dx.doi.org/10.1016/j.molcel.2012.07.014>.
- 44 39. Braukmann, F., Jordan, D., and Miska, E. (2017). Artificial and natural RNA interactions
45 between bacteria and *C. elegans*. *RNA Biol.* 14, 415–420. Available at:

- 1 <http://dx.doi.org/10.1080/15476286.2017.1297912>.
- 2 40. Nuez, I., and Félix, M.-A. (2012). Evolution of Susceptibility to Ingested Double-Stranded
3 RNAs in *Caenorhabditis* Nematodes. *PLoS One* 7, e29811. Available at:
4 <https://dx.plos.org/10.1371/journal.pone.0029811>.
- 5 41. Stefan, C., Jansen, S., and Bollen, M. (2005). NPP-type ectophosphodiesterases: Unity
6 in diversity. *Trends Biochem. Sci.* 30, 542–550.
- 7 42. Kato, K., Nishimasu, H., Okudaira, S., Mihara, E., Ishitani, R., Takagi, J., Aoki, J., and
8 Nureki, O. (2012). Crystal structure of Enpp1, an extracellular glycoprotein involved in
9 bone mineralization and insulin signaling. *Proc. Natl. Acad. Sci. U. S. A.* 109, 16876–
10 16881.
- 11 43. Roberts, F., Zhu, D., Farquharson, C., and Macrae, V.E. (2019). ENPP1 in the Regulation
12 of Mineralization and Beyond. *Trends Biochem. Sci.* 44, 616–628. Available at:
13 <https://doi.org/10.1016/j.tibs.2019.01.010>.
- 14 44. Onyedibe, K.I., Wang, M., and Sintim, H.O. (2019). ENPP1, an Old Enzyme with New
15 Functions, and Small Molecule Inhibitors—A STING in the Tale of ENPP1. *Molecules* 24,
16 4192. Available at: <https://www.mdpi.com/1420-3049/24/22/4192>.
- 17 45. Jin, Y., Cong, Q., Gvozdenovic-Jeremic, J., Hu, J., Zhang, Y., Terkeltaub, R., and Yang,
18 Y. (2018). Enpp1 inhibits ectopic joint calcification and maintains articular chondrocytes
19 by repressing hedgehog signaling. *Dev.* 145.
- 20 46. Coveney, C.R., Zhu, L., Miotla-Zarebska, J., Stott, B., Parisi, I., Batchelor, V., Duarte, C.,
21 Chang, E., McSorley, E., Vincent, T.L., *et al.* (2021). The ciliary protein IFT88 controls
22 post-natal cartilage thickness and influences development of osteoarthritis. *Arthritis*
23 *Rheumatol.*, 0–1.
- 24 47. Sonnevile, R., Querenet, M., Craig, A., Gartner, A., and Julian Blow, J. (2012). The
25 dynamics of replication licensing in live *Caenorhabditis elegans* embryos. *J. Cell Biol.*
26 196, 233–246.
- 27 48. Casar Tena, T., Maerz, L.D., Szafranski, K., Groth, M., Blätte, T.J., Donow, C., Matysik,
28 S., Walther, P., Jeggo, P.A., Burkhalter, M.D., *et al.* (2019). Resting cells rely on the DNA
29 helicase component MCM2 to build cilia. *Nucleic Acids Res.* 47, 134–151.
- 30 49. Gao, J., Wang, Q., Dong, C., Chen, S., Qi, Y., and Liu, Y. (2015). Whole exome
31 sequencing identified MCM2 as a novel causative gene for autosomal dominant
32 nonsyndromic deafness in a Chinese family. *PLoS One* 10, 75–80.
- 33 50. Razzauti, A., and Laurent, P.F. (2021). Ectocytosis prevents accumulation of ciliary cargo
34 in *C. elegans* sensory neurons. *Elife* 10. Available at:
35 <https://elifesciences.org/articles/67670>.
- 36 51. Gatti, J.L., Métayer, S., Belghazi, M., Dacheux, F., and Dacheux, J.L. (2005).
37 Identification, proteomic profiling, and origin of ram epididymal fluid exosome-like
38 vesicles. *Biol. Reprod.* 72, 1452–1465.
- 39 52. Mogielnicka-Brzozowska, M., Prochowska, S., Niżański, W., Bromke, M.A., Wiśniewski,
40 J., Olejnik, B., Kuzborska, A., Fraser, L., Młynarz, P., and Kordan, W. (2020). Proteome
41 of cat semen obtained after urethral catheterization. *Theriogenology* 141, 68–81.
- 42 53. Frenette, G., Girouard, J., D'Amours, O., Allard, N., Tessier, L., and Sullivan, R. (2010).
43 Characterization of two distinct populations of epididymosomes collected in the
44 intraluminal compartment of the bovine cauda epididymis. *Biol. Reprod.* 83, 473–480.
- 45 54. Kim, B., Suo, B., and Emmons, S.W. (2016). Gene Function Prediction Based on

- 1 Developmental Transcriptomes of the Two Sexes in *C. elegans*. *Cell Rep.* *17*, 917–928.
2 Available at: <http://dx.doi.org/10.1016/j.celrep.2016.09.051>.
- 3 55. Phiri, A.M., De Pomerai, D., Buttle, D.J., and Behnke, J.M.B. (2014). Developing a rapid
4 throughput screen for detection of nematicidal activity of plant cysteine proteinases: The
5 role of *Caenorhabditis elegans* cystatins. *Parasitology* *141*, 164–180.
- 6 56. Peracchi, A., Veiga-Da-Cunha, M., Kuhara, T., Ellens, K.W., Paczia, N., Stroobant, V.,
7 Seliga, A.K., Marlaire, S., Jaisson, S., Bommer, G.T., *et al.* (2017). Nit1 is a metabolite
8 repair enzyme that hydrolyzes deaminated glutathione. *Proc. Natl. Acad. Sci. U. S. A.*
9 *114*, E3233–E3242.
- 10 57. Stenvall, J., Fierro-González, J.C., Swoboda, P., Saamarthy, K., Cheng, Q., Cacho-
11 Valadez, B., Arnér, E.S.J., Persson, O.P., Miranda-Vizuete, A., and Tuck, S. (2011).
12 Selenoprotein TRXR-1 and GSR-1 are essential for removal of old cuticle during molting
13 in *Caenorhabditis elegans*. *Proc. Natl. Acad. Sci. U. S. A.* *108*, 1064–1069.
- 14 58. Liégeois, S., Benedetto, A., Garnier, J.M., Schwab, Y., and Labouesse, M. (2006). The
15 V0-ATPase mediates apical secretion of exosomes containing Hedgehog-related proteins
16 in *Caenorhabditis elegans*. *J. Cell Biol.* *173*, 949–961.
- 17 59. Kawasaki, I., Jeong, M.H., Yun, Y.J., Shin, Y.K., and Shim, Y.H. (2013). Cholesterol-
18 responsive metabolic proteins are required for larval development in *Caenorhabditis*
19 *elegans*. *Mol. Cells* *36*, 410–416.
- 20 60. Li, Y., Na, K., Lee, H.J., Lee, E.Y., and Paik, Y.K. (2011). Contribution of *sams-1* and
21 *pmt-1* to lipid homeostasis in adult *Caenorhabditis elegans*. *J. Biochem.* *149*, 529–538.
- 22 61. Loer, C.M., Davidson, B., and McKerrow, J. (1999). A phenylalanine hydroxylase gene
23 from the nematode *C. elegans* is expressed in the hypodermis. *J. Neurogenet.* *13*, 157–
24 180.
- 25 62. Loer, C.M., Calvo, A.C., Watschinger, K., Werner-Felmayer, G., O'Rourke, D., Stroud, D.,
26 Tong, A., Gotenstein, J.R., Chisholm, A.D., Hodgkin, J., *et al.* (2015). Cuticle integrity and
27 biogenic amine synthesis in *Caenorhabditis elegans* require the cofactor
28 tetrahydrobiopterin (BH4). *Genetics* *200*, 237–253.
- 29 63. Fisher, A.L., Page, K.E., Lithgow, G.J., and Nash, L. (2008). The *Caenorhabditis elegans*
30 *K10C2.4* gene encodes a member of the fumarylacetoacetate hydrolase family: A
31 *Caenorhabditis elegans* model of type I tyrosinemia. *J. Biol. Chem.* *283*, 9127–9135.
32 Available at: <http://dx.doi.org/10.1074/jbc.M708341200>.
- 33 64. Esposito, R., D'Aniello, S., Squarzone, P., Pezzotti, M.R., Ristatore, F., and Spagnuolo,
34 A. (2012). New insights into the evolution of metazoan tyrosinase gene family. *PLoS One*
35 *7*, 1–10.
- 36 65. Cohen, J.D., and Sundaram, M. V. (2020). *C. elegans* apical extracellular matrices shape
37 epithelia. *J. Dev. Biol.* *8*, 1–26.
- 38 66. Lažetić, V., and Fay, D.S. (2017). Molting in *C. elegans*. *Worm* *6*, e1330246. Available at:
39 <https://www.tandfonline.com/doi/full/10.1080/21624054.2017.1330246>.
- 40 67. Page, A. (2007). The cuticle. *WormBook*, 1–15. Available at:
41 http://www.wormbook.org/chapters/www_cuticle/cuticle.html.
- 42 68. Shurtleff, M.J., Temoche-Diaz, M.M., Karfilis, K. V., Ri, S., and Schekman, R. (2016). Y-
43 box protein 1 is required to sort microRNAs into exosomes in cells and in a cell-free
44 reaction. *Elife* *5*, 1–23.
- 45 69. Arnold, A., Rahman, M.M., Lee, M.C., Muehlhaeusser, S., Katic, I., Gaidatzis, D., Hess,

- 1 D., Scheckel, C., Wright, J.E., Stetak, A., *et al.* (2014). Functional characterization of *C.*
2 *elegans* Y-box-binding proteins reveals tissue-specific functions and a critical role in the
3 formation of polysomes. *Nucleic Acids Res.* *42*, 13353–13369.
- 4 70. Youngman, E.M., and Claycomb, J.M. (2014). From early lessons to new frontiers: The
5 worm as a treasure trove of small RNA biology. *Front. Genet.* *5*, 1–13.
- 6 71. Sundby, A.E., Molnar, R.I., and Claycomb, J.M. (2021). Connecting the Dots: Linking
7 *Caenorhabditis elegans* Small RNA Pathways and Germ Granules. *Trends Cell Biol.* *31*,
8 387–401. Available at: <https://doi.org/10.1016/j.tcb.2020.12.012>.
- 9 72. Russell, J.C., Kim, T.K., Noori, A., Merrihew, G.E., Robbins, J.E., Golubeva, A., Wang,
10 K., MacCoss, M.J., and Kaerberlein, M. (2020). Composition of *Caenorhabditis elegans*
11 extracellular vesicles suggests roles in metabolism, immunity, and aging. *GeroScience*
12 *42*, 1133–1145.
- 13 73. Duguet, T.B., Soichot, J., Kuzyakiv, R., Malmström, L., and Tritten, L. (2020).
14 Extracellular Vesicle-Contained microRNA of *C. elegans* as a Tool to Decipher the
15 Molecular Basis of Nematode Parasitism. *Front. Cell. Infect. Microbiol.* *10*, 1–11.
- 16 74. Sharma, U., Sun, F., Conine, C.C., Reichholf, B., Kukreja, S., Herzog, V.A., Ameres, S.L.,
17 and Rando, O.J. (2018). Small RNAs Are Trafficked from the Epididymis to Developing
18 Mammalian Sperm. *Dev. Cell* *46*, 481-494.e6. Available at:
19 <https://doi.org/10.1016/j.devcel.2018.06.023>.
- 20 75. Shi, C., and Murphy, C.T. (2020). Sex and death. *Curr. Top. Dev. Biol.*, 353–375.
- 21 76. Drurey, C., Coakley, G., and Maizels, R.M. (2020). Extracellular vesicles: new targets for
22 vaccines against helminth parasites. *Int. J. Parasitol.* *50*, 623–633. Available at:
23 <https://doi.org/10.1016/j.ijpara.2020.04.011>.
- 24 77. Morsci, N.S., and Barr, M.M. (2011). Kinesin-3 KLP-6 regulates intraflagellar transport in
25 male-specific cilia of *caenorhabditis elegans*. *Curr. Biol.* *21*, 1239–1244. Available at:
26 <http://dx.doi.org/10.1016/j.cub.2011.06.027>.
- 27 78. Brenner, S. (1974). The genetics of *Caenorhabditis elegans*. *Genetics* *77*, 71–94.
- 28 79. Granato, M., Schnabel, H., and Schnabel, R. (1994). *pha-1*, a selectable marker for gene
29 transfer in *C.elegans*. *Nucleic Acids Res.* *22*, 1762–1763.
- 30 80. Craig, R., and Beavis, R.C. (2004). TANDEM: Matching proteins with tandem mass
31 spectra. *Bioinformatics* *20*, 1466–1467.
- 32 81. Gupta, N., Bandeira, N., Keich, U., and Pevzner, P.A. (2011). Target-decoy approach and
33 false discovery rate: When things may go wrong. *J. Am. Soc. Mass Spectrom.* *22*, 1111–
34 1120.
- 35 82. Zhang, X., Smits, A.H., Van Tilburg, G.B.A., Ovaa, H., Huber, W., and Vermeulen, M.
36 (2018). Proteome-wide identification of ubiquitin interactions using UblA-MS. *Nat. Protoc.*
37 *13*, 530–550. Available at: <http://dx.doi.org/10.1038/nprot.2017.147>.
- 38 83. Ritchie, M.E., Phipson, B., Wu, D., Hu, Y., Law, C.W., Shi, W., and Smyth, G.K. (2015).
39 limma powers differential expression analyses for RNA-sequencing and microarray
40 studies. *Nucleic Acids Res.* *43*, e47–e47. Available at:
41 [http://academic.oup.com/nar/article/43/7/e47/2414268/limma-powers-differential-](http://academic.oup.com/nar/article/43/7/e47/2414268/limma-powers-differential-expression-analyses-for)
42 [expression-analyses-for](http://academic.oup.com/nar/article/43/7/e47/2414268/limma-powers-differential-expression-analyses-for).
- 43 84. Dokshin, G.A., Ghanta, K.S., Piscopo, K.M., and Mello, C.C. (2018). Robust Genome
44 Editing with Short Single-Stranded. *Genetics* *210*, 781–787.

1 85. Peterson, B.G., and Carl, P. (2020). PerformanceAnalytics: Econometric Tools for
2 Performance and Risk Analysis. Available at: [https://cran.r-](https://cran.r-project.org/package=PerformanceAnalytics)
3 [project.org/package=PerformanceAnalytics](https://cran.r-project.org/package=PerformanceAnalytics).

4 86. Lints, R., and Hall, D.H. Male alimentary system, proctodeum. WormAtlas.

5 **Acknowledgments:** We are grateful to Haiyan Zheng for assistance with the mass
6 spectrometry analysis, Gloria Androwski and Helen Ushakov for outstanding technical
7 assistance, Piali Sengupta, Rachel Kaletsky, Coleen Murphy, Julie Claycomb, and Tetsuya
8 Nakamura for discussions, and members of the Boston and UCSF cilia supergroups and
9 Rutgers *C. elegans* community for thought-provoking questions. We also thank WormBase
10 (release WS281), WormAtlas, and WormBook that were used daily during this project.

11 **Funding:** The work was funded by grants from the National Institutes of Health (NIH)
12 DK116606 and DK059418 to M.M.B, K12 GM093854 to J.D.W. Protein identification was
13 performed in the Biological Mass Spectrometry Facility of Robert Wood Johnson Medical School
14 at Rutgers University supported by the NIH instrumentation grants S10OD025140 and
15 S10OD016400. Some strains were provided by the Caenorhabditis Genetics Center (CGC),
16 which is funded by NIH Office of Research Infrastructure Programs (P40 OD010440).

17 **Author contributions:**

18 Conceptualization: IAN, JW, MMB

19 Methodology: IAN, JW, JDW, ALC, PT, PS

20 Investigation: IAN, JW, KMP, JSA, ALC

21 Visualization: IAN, JW, KMP, JSA, PT

22 Funding acquisition: MMB, JDW, PS

23 Project administration: IAN, JW, MMB, PS

24 Supervision: MMB, PS

25 Writing – original draft: IAN

26 Writing – review & editing: IAN, JW, ALC, KMP, JDW, JSA, ARK, PS, MMB

27 **Competing interests:** Authors declare that they have no competing interests.

28 **Data and materials availability:** Raw proteomics data generated in this study are available
29 at <https://massive.ucsd.edu/> (Accession number - MSV000087943). Generated plasmids
30 and animal strains are available upon request.

31 **Supplementary Materials**

32 Materials and Methods

33 Figs. S1 to S12

34 Tables S1 to S3

35 Movies S1 to S2

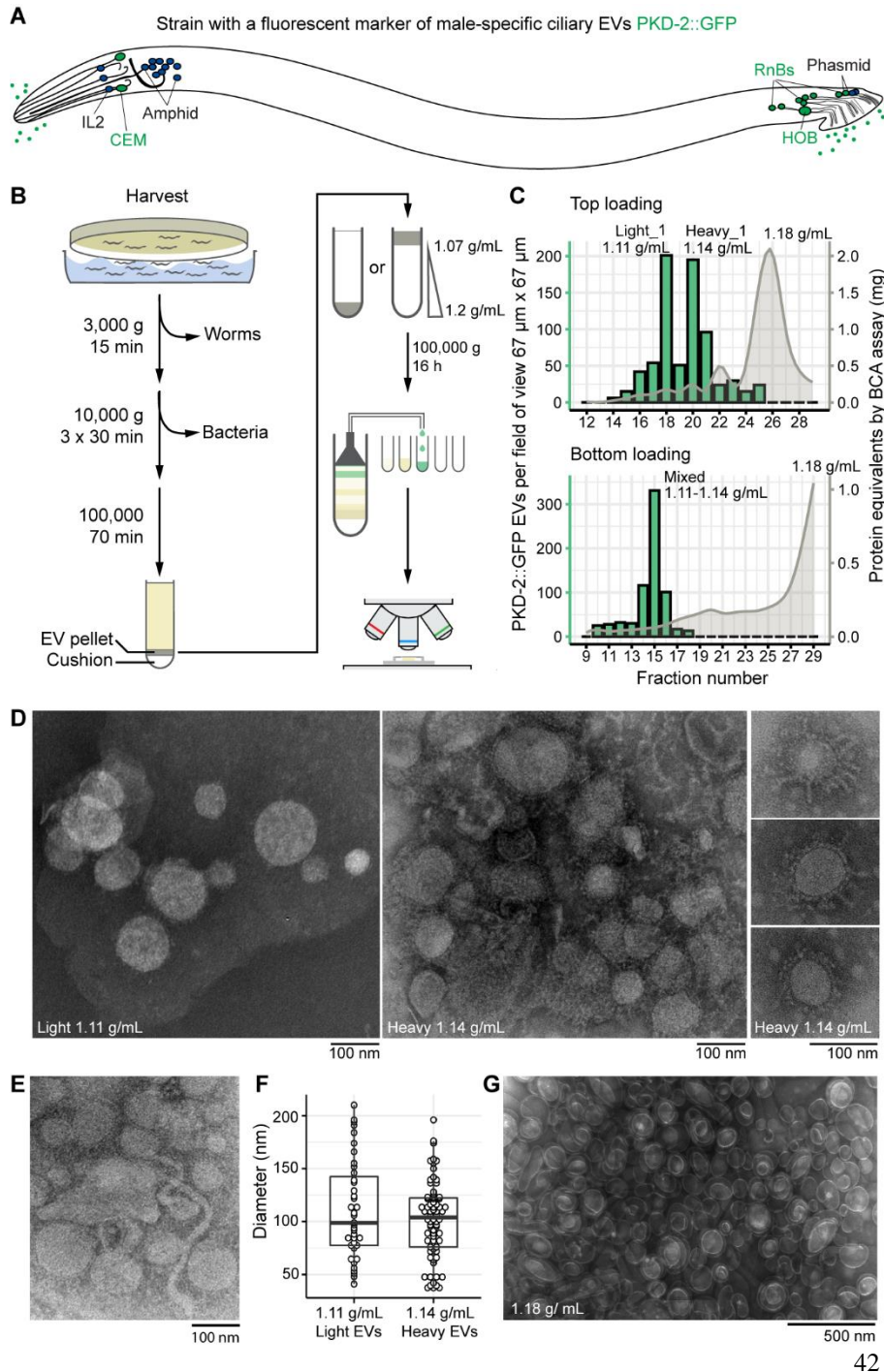


Figure 1. Buoyant density centrifugation enriches for ciliary PKD-2::GFP EVs more than 100-fold and resolves them into two populations. (A)

Location of environmentally exposed cilia of sensory neurons. Male-specific cilia are labeled in green.

Neurons: CEM – cephalic male, IL2 – inner labial type 2, HOB – hook type B, RnBs – ray neurons type B. (B) Schematic of the EV enrichment workflow. (C)

Combination charts showing number of the PKD-2::GFP EVs and the amount of protein in the collected fractions. Centrifugation of the top-loaded sample resolved PKD-2 EVs in two types with densities 1.11 g/ml (light) and 1.14 g/mL (heavy), respectively.

Bottom-loaded samples failed to resolve the PKD-2 EV subtypes but reached a similar level of enrichment (more than 100-fold). (D)

Transmission electron microscopy (TEM) of the negatively stained PKD-2 EV enriched fractions revealed presence of vesicles with coatings.

43 (E) Tubular structures of 17-20 nm in diameter reminiscent of the stem of a budding vesicle. (F)

44 Diameters of EVs recovered from the light and heavy fractions fall in the range of 50 - 200 nm

45 as measured by TEM. (G) EVs from the fraction with most protein, presumably bacterial OMVs.

46

1 Table S2). **(C)** Identified EVome contained proteins encoded by previously identified transcripts
2 specific to EV-releasing neurons (EVNs). The Venn diagram shows EV cargo candidates that
3 overlap with two transcriptomic datasets [10,31]. **(D)** GFP::**KLP-6** EV shedding from the IL2 cilia
4 of a wild-type hermaphrodite, orthogonal projection. GFP::**KLP-6** was observed in EVs released
5 outside the animal. **(E)** The transcriptome of EV-releasing neurons is most similar to the
6 Cholinergic cluster 15 from [37] likely representing the IL2 neurons. **(F)** EV cargo candidates
7 were categorized into three groups based on their relative enrichment in the IL2 sex-shared EV-
8 releasing neurons (x-axis) and in the ciliated neurons (y-axis). Three categories are indicated by
9 colors. Previously validated ciliary EV cargoes are bolded.

10

11

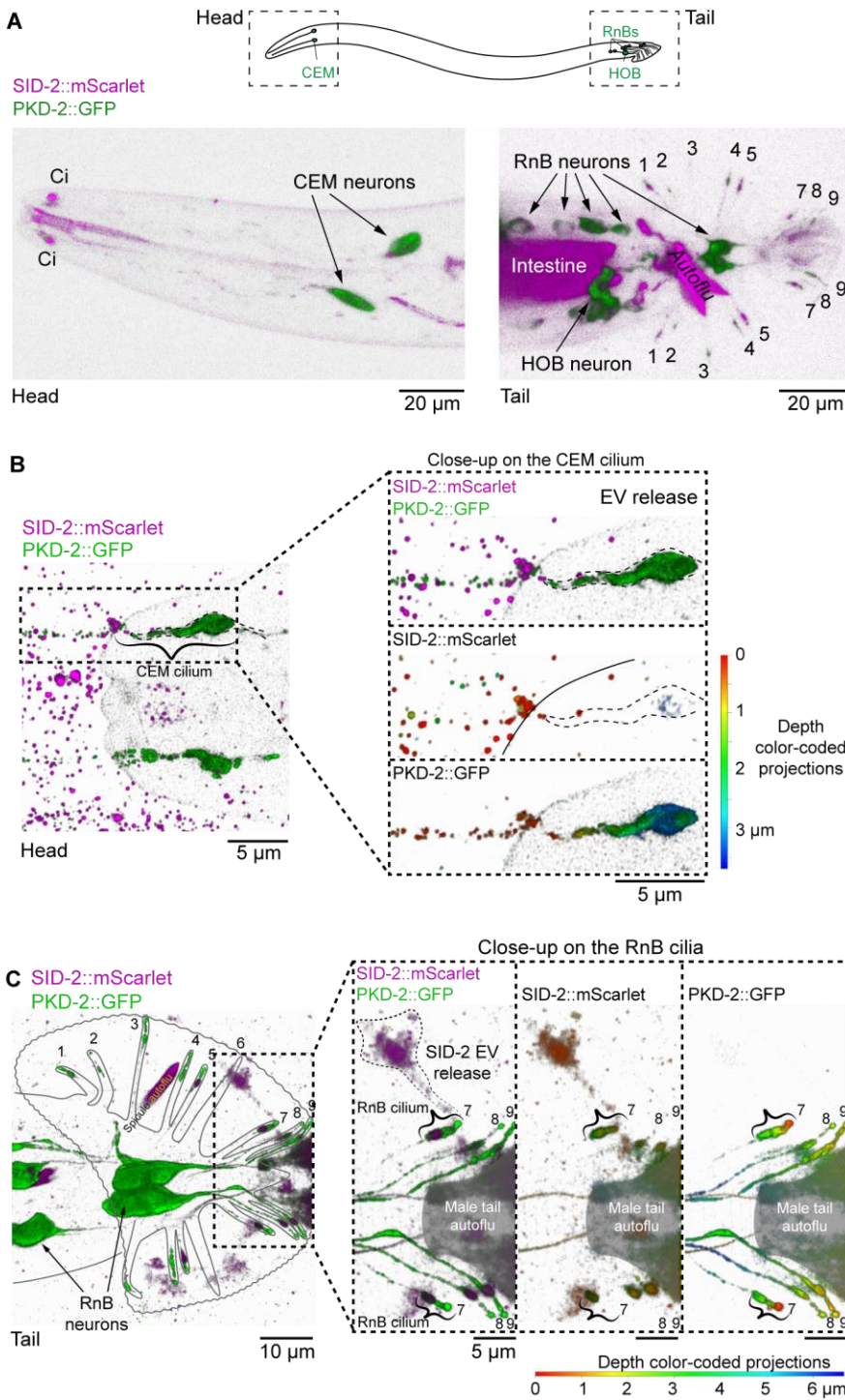
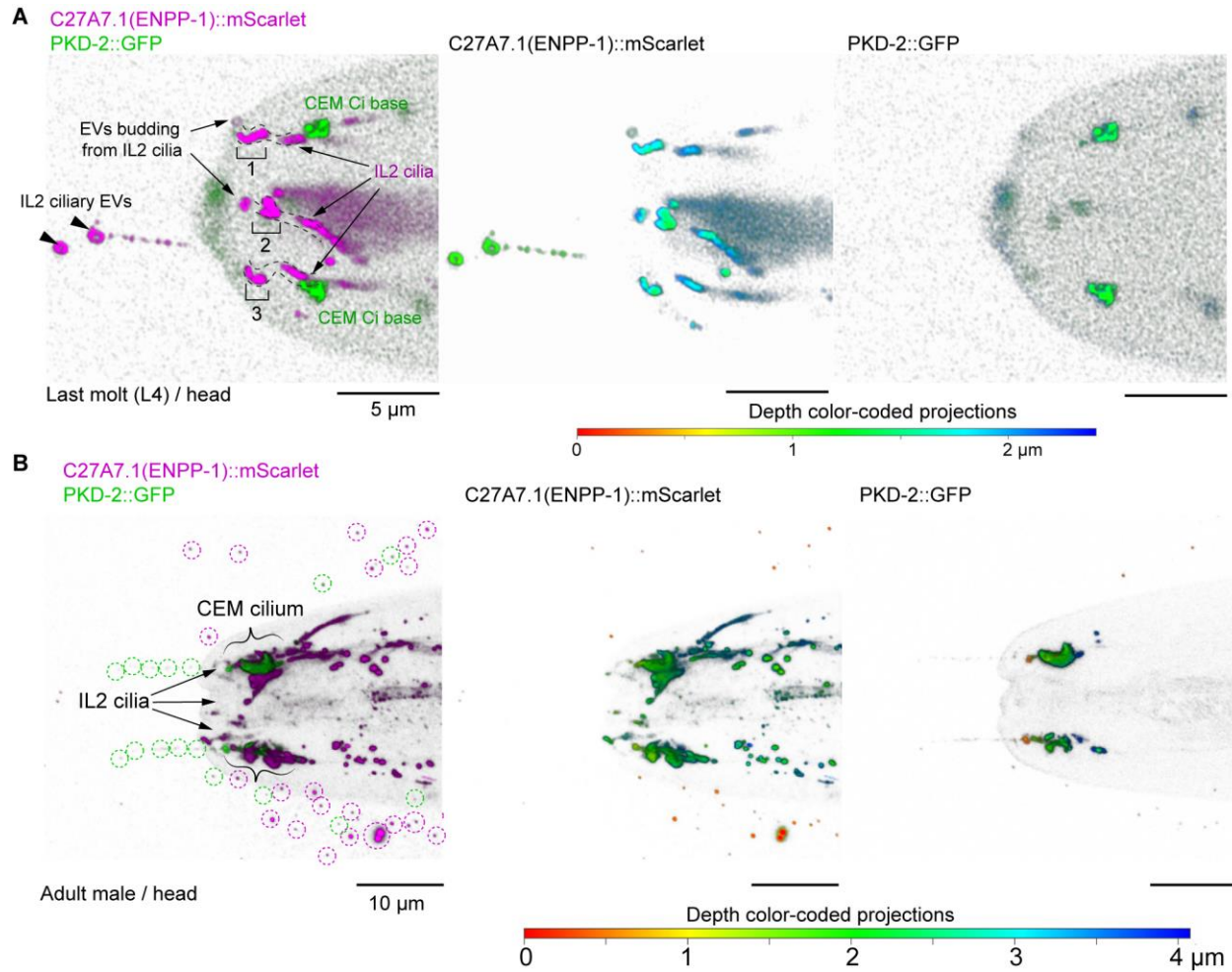


Figure 3. Nucleic acid binding transporter SID-2 is specifically enriched in the male-specific ciliated EV-releasing neurons (EVNs) and is shed in the form of EVs to the environment. (A-C) SID-2::mScarlet and PKD-2::GFP reporter presence in the head and tail of an adult male. Zoomed insets in (B) and (C) show ciliary localization and EV release. Areas of intense inherent autofluorescence are shaded with gray and labeled as autoflu. Cilia, CEM – cephalic male neuron, HOB – hook neuron type B, RnB – Ray neuron type B. Merged images are shown as 3D projections; individual channels are presented as depth color-coded projections with minimal labeling where colocalized presence is indicated by the same color (such as SID-2 and PKD-2 presence within the CEM cilium in (B) is indicated with blue which corresponds to ~3.5 μm distance deep into the acquired Z-stack). For individual channels of (A) see Figure S3.



1
2 **Figure 4. Phosphodiesterase ENPP-1 is a ciliary EV cargo.** Ciliary localization of ENPP-
3 1::mScarlet in the sensory neurons of the head: IL2 (**A**) and CEM (**B**). IL2 EVs are indicated by
4 arrowheads, CEM EVs are shown by dashed circles. See movie S1 for time-lapse imaging of
5 ENPP-1::mScarlet ectocytosis from IL2 cilia. PKD-2::GFP served as a marker of the CEM cilia
6 and EVs.

7

8

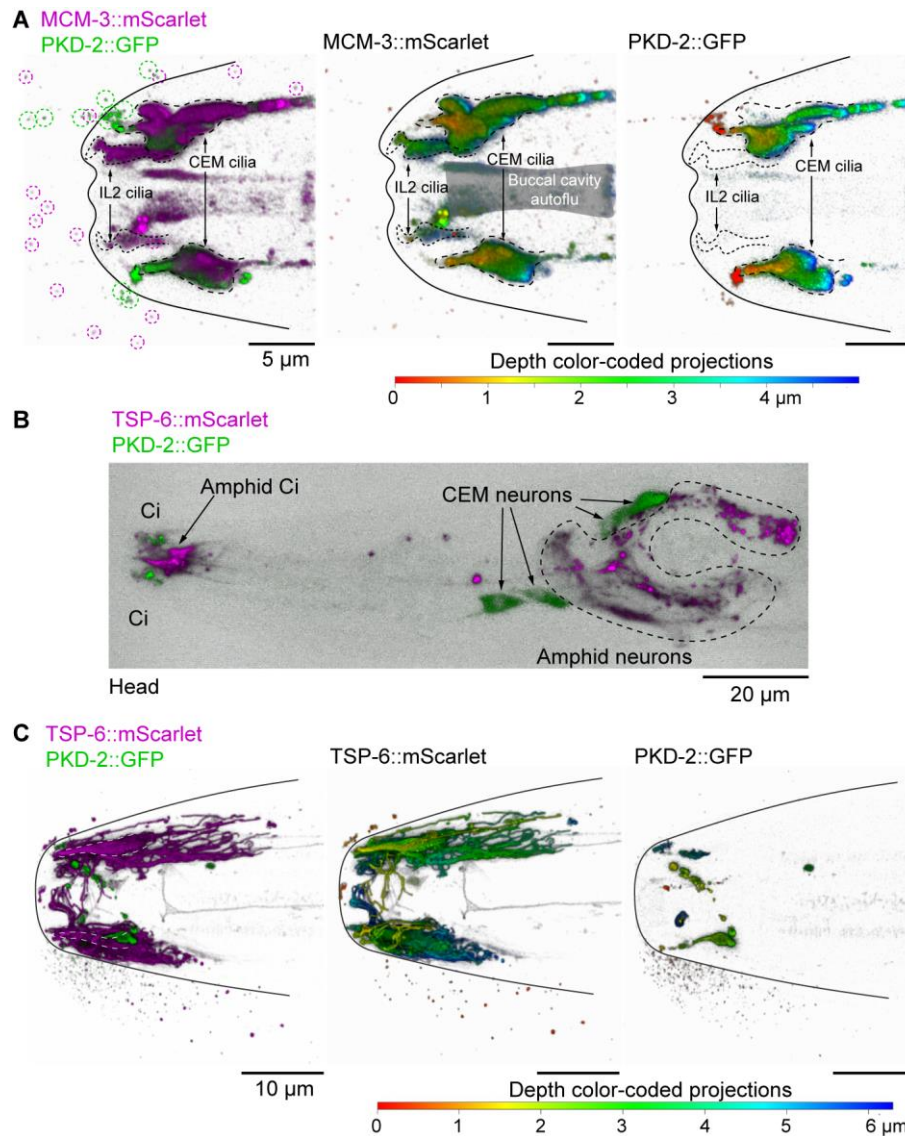


Figure 5. Different neuronal types carry distinct EV cargo; a single neuronal cilium may shed multiple cargoes. (A) MCM-3::mScarlet is present in cilia of PKD-2-expressing and IL2 neurons. Circles indicate MCM-3::Scarlet (magenta) and PKD-2::GFP EVs **(B-C)** TSP-6::mScarlet is present in amphid channel and AWA neurons of the head (C) and is released in ciliary EVs into the environment (D). Amphid channel is outline with white dashed line. Merged 3D projections are shown; individual channels are presented as depth color-coded projections with minimal labeling.

1 Materials and Methods

2 Strains

Name	Genotype	Purpose
PT3112	<i>pha-1(e2123ts) III; him-5(e1490) myls4[pkd-2p::pkd-2::gfp + unc-122p::GFP] V; myEx888 [Pcil-7::cil-7::tagrfp + pBX1]</i>	EV isolation [13]
PT2102	<i>pha-1(e2123) III; him-5(e1490) V; myEx686 [klp-6p::gfp::klp-6::3'UTR + pBX1]</i>	EV cargo validation [77]
PT3545	<i>pha-1 (e2123ts) III; myls1 [pkd-2p::pkd-2::gfp + unc-122p::GFP] IV; him-5 (e1490) V; myEx944[tsp-6p::tsp-6::mScarlet 20 ng/ul + pBX1 100 ng/ul]</i>	EV cargo validation
PT3562	<i>sid-2 (my95[sid-2::mScarlet]) III; myls4[pkd-2p::pkd-2::gfp + unc-122p::GFP] him-5 (e1490) V.</i>	EV cargo validation
PT3617	<i>pha-1 (e2123ts) III; myls1 [pkd-2p::pkd-2::gfp + unc-122p::GFP] IV; him-5 (e1490) V; myEx951[mcm-3p::mcm-3::mScarlet 20 ng/ul + pBX1 100 ng/ul]</i>	EV cargo validation
PT3618	<i>pha-1 (e2123ts) III; myls1 [pkd-2p::pkd-2::gfp + unc-122p::GFP] IV; him-5 (e1490) V; myEx948[c27a7.1p::c27a7.1::mScarlet 20 ng/ul + pBX1 100 ng/ul]</i>	EV cargo validation

3

4 General maintenance of *C. elegans*

5 Animals were routinely maintained on 6-cm plates with normal growth medium (NGM) (3 g of
6 NaCl, 2.5 g of peptone, and 20 g of agar per 1 L) seeded with 100 μ L *E. coli* strain OP50 [78].
7 Wild-type strains were propagated at 20°C, whereas temperature sensitive strains carrying *pha-*
8 *1 (e2123 ts)* alleles were grown at 15°C up until their transgenesis with a cocktail containing a
9 functional *pha-1* allele. After that, the transgenic animals were transferred to a restrictive
10 temperature of 22°C to select for animals carrying the transgene-of-interest [79].

11 Propagation of *C. elegans* for EV enrichment

12 To initiate the culture, 180 hermaphrodites were transferred to 30 6-cm NGM plates (6 animals
13 per plate) and grown for 2 generations. At day 6, each plate was chunked into quarters and the
14 chunks were transferred into 15-cm plates with high growth medium (HGM) (3 g of NaCl, 2.5 g
15 of peptone, and 20 g of agar per 1 L supplemented with 4 mL of cholesterol stock (5 mg/mL of
16 ethanol), 1 mL 1M CaCl₂, 1 mL 1M MgSO₄, and 25 mL 1M potassium phosphate buffer pH 6.0)
17 seeded with a full lawn of *E. coli* OP50 (1.8 mL/plate). Animals were allowed to propagate for 2
18 more generations until almost all bacteria were consumed, yet animals were not starved.

19 *C. elegans* harvest and EV enrichment procedure

20 Animals were collected into a shallow dish with the M9 buffer (3 g KH₂PO₄, 6 g Na₂HPO₄, 5 g
21 NaCl, 1 ml 1 M MgSO₄ per 1 L of ultrapure water) by inverting the 15-cm plates and their gentle
22 agitation against the surface of the buffer. A total of 200 mL of M9 buffer was used to release
23 worms from 30 HGM plates. The collected worm suspension was centrifuged at 3,000 g for 15
24 minutes at 15°C in 15 mL conical tubes to pellet the worms and bacteria. The supernatant was
25 transferred to fresh tubes and centrifuged at 10,000 g for 30 minutes 3 times at 4°C (in SS34
26 fixed angle rotor) to get rid of residual bacteria. Cleared supernatants were then transferred to
27 fresh 12 mL Beckman Coulter round bottom tubes and layered with a 2 mL 36% iodixanol

1 cushion. The cushion was prepared by mixing 3 parts of 60% iodixanol (OptiPrep, Sigma
2 #D1556) and 2 parts of 8% sucrose to achieve final density of 1.2 g/L. EVs were collected onto
3 the cushion via centrifugation in the SW41 Ti swinging bucket rotor at 30,000 rpm (110,000 g
4 average) for 70 minutes at 4°C. EV pellets were collected with a thin glass Pasteur pipette, and
5 further diluted either with M9 buffer to a final density of less than 1.07 g/mL for top loading or
6 with 60% iodixanol to final density of 1.18 g/mL for bottom loading. The gradients were prepared
7 ahead of time by a freeze-thaw method. Specifically, 12%, 16%, 20%, 24%, 28%, and 32%
8 iodixanol solutions were made by mixing solution A (8% sucrose) with solution B (60%
9 iodixanol) so that final osmolarities ranged from 270 to 320 mOsm and densities ranged from
10 1.08 to 1.20 g/mL. The solutions were then layered in a stepwise manner starting from the
11 heaviest layer and freezing the content at -80°C after each added layer. The gradients were
12 thawed at room temperature 1-2 hours prior to use and remained at 4°C up until loading.
13 Loading was performed using a glass Pasteur pipette. Isopycnic centrifugation was carried out
14 for 16 hours at 30,000 rpm using the SW41 Ti Beckman Coulter rotor at 4°C. Fractions were
15 collected using the BioComp's Piston Gradient Fractionator. Aliquots were taken from each
16 fraction to measure density, protein concentration, and examine enrichment with PKD-2::GFP-
17 carrying EVs. Density was measured by weighing out 150 µL of the examined solution on an
18 analytical scale to calculate weight per volume ratio for each fraction. Protein concentration was
19 measured using Bicinchoninic Acid (BCA) Protein Assay Kit (Pierce, Thermo Fisher #23225)
20 according to manufacturer's instructions in the presence of 0.2% SDS. PKD-2::GFP EV
21 enrichment was assessed by scanning through an array of representative droplets from each
22 fraction using a Zeiss LSM 880 confocal microscope and its Airyscan detector. Once the most
23 enriched fractions were identified, total protein was isolated from them via methanol-chloroform
24 extraction. Briefly, four volumes of methanol were added to one volume of the EV-enriched
25 fraction, vortexed vigorously for 10 seconds, followed by addition of one volume of chloroform
26 and repeated intense vortexing, followed by addition of three volumes of ultrapure water and
27 vortexing. Phase separation was completed by centrifugation at 16,000 g in a tabletop
28 centrifuge for 1 minute. The aqueous upper layer was discarded without disturbing the white
29 flaky proteinaceous interphase. Protein was precipitated by adding four volumes of methanol
30 and centrifugation at 16,000 g for 10 minutes. Protein pellets were dried and dissolved in 2x
31 Laemmli buffer (0.125 M Tris HCl pH6.8, 4% SDS, 20% glycerol, 10% 2-mercaptoethanol,
32 0.004% bromophenol blue) at 90°C for 5 minutes. Resulting proteins were analyzed by
33 denaturing electrophoresis in polyacrylamide gel (SDS-PAGE) or sent for protein identification
34 by mass spectrometry.

35 Transmission electron microscopy

36 Fractions most enriched with PKD-2::GFP carrying EVs were diluted 10-20 times with M9 buffer
37 and applied to discharged formvar/carbon coated copper grids (200 mesh, Electron Microscopy
38 Sciences # FCF200-Cu). Five microliters of the diluted fraction were dispensed on the grid and
39 allowed on for 30-60 seconds followed by wicking the liquid away from the grid with Whatman
40 filter paper #1. The grid was then transferred through 3 droplets of PBS (5 min in each droplet)
41 to wash away residual sucrose and iodixanol. The excess of PBS was wicked away with the
42 filter paper after each wash. For the unfixed preparation, following PBS washes the grid was
43 exposed to the Nano-W stain (Methylamine Tungstate solution, Nanoprobes #2018) for 1
44 minute sharp. The stain was removed with the filter paper and the grid was left to dry out
45 completely for 30 minutes at room temperature. Imaging was performed on Philips CM12
46 electron microscope with AMT-XR11 digital camera. Best results were achieved with imaging
47 the samples on the day of their staining.

48 Liquid chromatography-tandem mass spectrometry (LC-MS-MS)

1 Samples were allowed to run in an acrylamide gel for a distance of 3-5 cm. Regions-of-interest
2 were excised for further protein processing. Each piece was subjected to reduction with 10 mM
3 dithiothreitol for 30 min at 60°C, alkylation with 20 mM iodoacetamide for 45 min at room
4 temperature in the dark, and digestion with sequencing grade trypsin (Thermo Scientific
5 #90058) overnight at 37°C. Peptides were extracted twice with 5% formic acid, 60% acetonitrile
6 and dried under vacuum.

7 Samples Light_1 and Heavy_1 were analyzed using Dionex UltiMate 3000 RLSCnano System,
8 ThermoFisher) interfaced with QExactive HF (ThermoFisher). Samples were loaded onto a
9 fused silica trap column Acclaim PepMap 100, 0.075 mm x 200 mm (ThermoFisher). After
10 washing for 5 min at 5 µl/min with 0.1% trifluoroacetic acid, the trap column was brought in-line
11 with an analytical column (nanoEase M/Z Peptide BEH C18 column, 130 Å, 1.7 µm, 0.075 mm x
12 250 mm, Waters) for LC-MS-MS. Peptides were fractionated at 300 nL/min using a segmented
13 linear gradient of 4-15% solution “B” in solution “A” for 30 min (where A is a polar solvent 0.2%
14 formic acid, and B is an organic solvent of 0.16% formic acid and 80% acetonitrile), 15-25% for
15 40 min, 25-50% for 44 min, and 50-90% B for 11 min. The column was re-equilibrated with 4%
16 solution “B” in solution “A” for 5 minutes prior to the next run. Cyclic series of full scan acquired
17 in Orbitrap with resolution of 120,000 were followed by MS-MS (HCD relative collision energy
18 27%) of the 20 most intense ions at resolution 30,000 and dynamic exclusion duration of 20 sec.

19 For the samples Mixed, Light_2, Heavy_2, Light_3, Heavy_3, Light_4, Heavy_4, Light_5,
20 Heavy_5, Light_6, Light_7, Heavy_6, LC-MSMS were done using Dionex UltiMate 3000
21 RLSCnano System interfaced with Eclipse Orbitrap tribrid (ThermoFisher). The LC method is
22 the same as described above. For mass spectrometry, the scan sequences began with MS1
23 spectrum (Orbitrap analysis, resolution 120,000, scan range from M/Z 375–1500, automatic
24 gain control (AGC) target 1E6, maximum injection time 100 ms). The top S (3 sec) and dynamic
25 exclusion of 60 sec were used for selection of parent ions of charge 2-7 for MS-MS. Parent
26 masses were isolated in the quadrupole with an isolation window of 1.2 m/z, AGC target 1E5,
27 and fragmented with higher-energy collisional dissociation with a normalized collision energy of
28 30%. The fragments were scanned in Orbitrap with resolution of 15,000. The MS-MS scan
29 range were determined by charge state of the parent ion but lower limit was set at 110 amu.

30

31 Protein identification

32 The peak list of the LC-MS-MS were generated by Thermo Proteome Discoverer (v. 2.1) into
33 MASCOT Generic Format (MGF) and searched against databases of *C. elegans* (Ensembl), *E.*
34 *coli* K12 substrain MG1655 (NCBI), and Contaminant Repository for Affinity Purification Mass
35 Spectrometry Data (CRAP) using in house version of X!Tandem GPM (The Global Proteome
36 Machine) Fury [80]. Search parameters were as follows: fragment mass error 20 ppm, parent
37 mass 5 error +/- 7 ppm, fixed modification - carbamidomethylation on cysteine, variable
38 modifications - oxidation on methionine, protease specificity - trypsin (C-terminal of R/K unless
39 followed by P), with 1 miss-cut at preliminary search and 5 miss-cuts during refinement. To
40 validate the protein and peptides, false positive rate (FPR) [81] value was used to decide the
41 log(e) cutoff. Only spectra with log(e) < -2 were included in the final report.

42 Analysis of differential abundance in light vs. heavy fractions

43 For the differential abundance analysis, the “Mixed” dataset was omitted as these EVs did not
44 resolve in two populations. For the rest of the samples Normalized Spectral Abundance Factors
45 (NSAFs) were calculated from uniquely mapped spectral counts. Batch corrections were applied
46 using the R package msmsEDA. For differential expression analysis, we considered only
47 proteins that were identified in more than one replicate for both heavy and light subpopulations.
48 For these proteins, missing values were imputed using the QRILIC method as implemented in
49 the R package DEP [82]. Differential expression analysis was performed using the R package

1 limma [83], using the trend and robust hyperparameter estimation settings. P-values were
2 adjusted using the Benjamini-Hochberg procedure. Proteins were considered differentially
3 expressed between the heavy and light EVs if they had an absolute log₂ fold changes greater or
4 equal to 1.5 and an adjusted p-value < 0.05.

5 Gene ontology and InterPro enrichment

6 KEGG enrichment was performed using clusterProfiler R package. KEGG enrichment in the
7 heavy EVs included proteins that were upregulated relative to the light EVs and those proteins
8 only detected in the heavy EVs. A similar procedure was performed for light EVs. The
9 background for KEGG enrichments of differentially abundant proteins included only proteins
10 detected via LC-MS-MS. InterPro domain enrichment was performed using a hypergeometric
11 test in a custom R script, with p-values corrected using the Benjamini-Hochberg procedure.

12 Coupling the mass spectrometry data with single cell transcriptomics of *C. elegans*

13 EV cargo were assigned scores derived from single-cell transcriptomics datasets [37].
14 Enrichment in ciliated neurons was calculated as the ratio of transcript abundance (transcript
15 per million, TPM) in ciliated neurons over mean transcript abundance across all the tissues.
16 Enrichment in IL2 neurons was calculated as the ratio of transcript abundance in IL2 neurons
17 over its mean abundance in all neurons. Identity of the IL2 neurons was established as
18 Cholinergic clusters 15 from [37] based on similarities of their transcriptional profiles to the list of
19 transcripts enriched in the EV-releasing neurons identified in [10]. The similarity was determined
20 by hierarchical clustering analysis of the fold change enrichment values of EVN-specific
21 transcripts from [10] to the fold change enrichment of respective cholinergic neurons transcripts
22 over all identified cholinergic neuronal clusters of *C. elegans*. The values that were used for
23 generation of the dendrogram on Figure 2E are indicated in Supplemental table S3.

24 Transgenesis for EV cargo validation

25 Pieces of genomic DNA were cloned into the vector backbone encoding the C-terminally linked
26 flexible linker (amino acid sequence is GGGSGGGSGGGSGGG) fused to the mScarlet coding
27 sequence and *unc-54* 3'UTR using the following primers (annealing regions only are indicated
28 to orient the reader on which genomic piece was cloned):
29

Transgene	Promoter	Primer annealing regions used for cloning
<i>mcm-3p::mcm-3::mScarlet</i>	1005	Fw: 5'-ATCTGAATACTACAGTACTCCTTAAAGGTG-3' Rv: 5'-GATGAGAGTGATCTTATCTTCGGCA-3'
<i>c27a7.1p::C27A7.1::mScarlet</i>	1174	Fw: 5'-CGGAGATGTGCAGTAACTACTG-3' Rv: 5'-CCAGAGTTTTGTAGATATCTTCCTTCTA-3'
<i>tsp-6p::tsp-6::mScarlet</i>	2017	Fw: 5'-GTTTTGTCACTTTTTGGATCAAAATTTGTTCAATTG-3' Rv: 5'-AGCTTGGGAGCGTTTCTCTTTGAC-3'

30 All the transgenes were fully sequenced prior to transgenesis. Respective plasmids were
31 injected with a co-injection selective marker *pha-1(+)* into *pha-1 (e2123 temperature sensitive)*
32 *III; him-5 V* strain. Further maintenance of the transgenic worms at 22°C ensured selection for
33 and retention of the extrachromosomal transgenic arrays.

34 The *sid-2::mScarlet* reporter was generated using CRISPR/Cas9-mediated editing as
35 described in [84] using a guide RNA (5'-CCTTCGCTACATTGGAAAGC-3') and a double
36 stranded DNA donor template containing a sequence encoding the flexible linker of 15 amino
37 acids (GGGS)₃ fused to the mScarlet coding sequence (Figure S3A). The mScarlet coding
38 sequence was intron-less to not interfere with native splicing regulation within the *dyf-2* gene.

39 Mounting animals for super resolution live animal imaging

40 Animals were anesthetized with 10 mM levamisole solution in the M9 buffer. To completely
41 immobilize the worm, we used thin agarose pads, prepared from 10% melted agarose (Sigma

1 #A9539) and ultrapure water. Melting of the 10% agarose was achieved by pulse heating in a
2 microwave in 3 second intervals for a total of 1 minute or until dry agarose pieces were no
3 longer visible. Once melted, the 10% agarose was incubated at 95°C for about 10 minutes to
4 allow air bubbles to escape. The melted agarose was dispensed onto glass slides in 100 μ L
5 droplets and the droplets were immediately pressed with a second glass slide to make a thin gel
6 pad. The agarose pads were made in batches and stored in a sealed glass slide container at
7 room temperature for up to a week. Animals were mounted by their placement in 1 μ L droplet of
8 10 mM levamisole dispensed on a 18 x 18 cm coverslip, followed by flipping of the coverslip
9 onto the center of the agarose pad. Animals were imaged within 30 minutes of their mounting.

10 Super-resolution microscopy

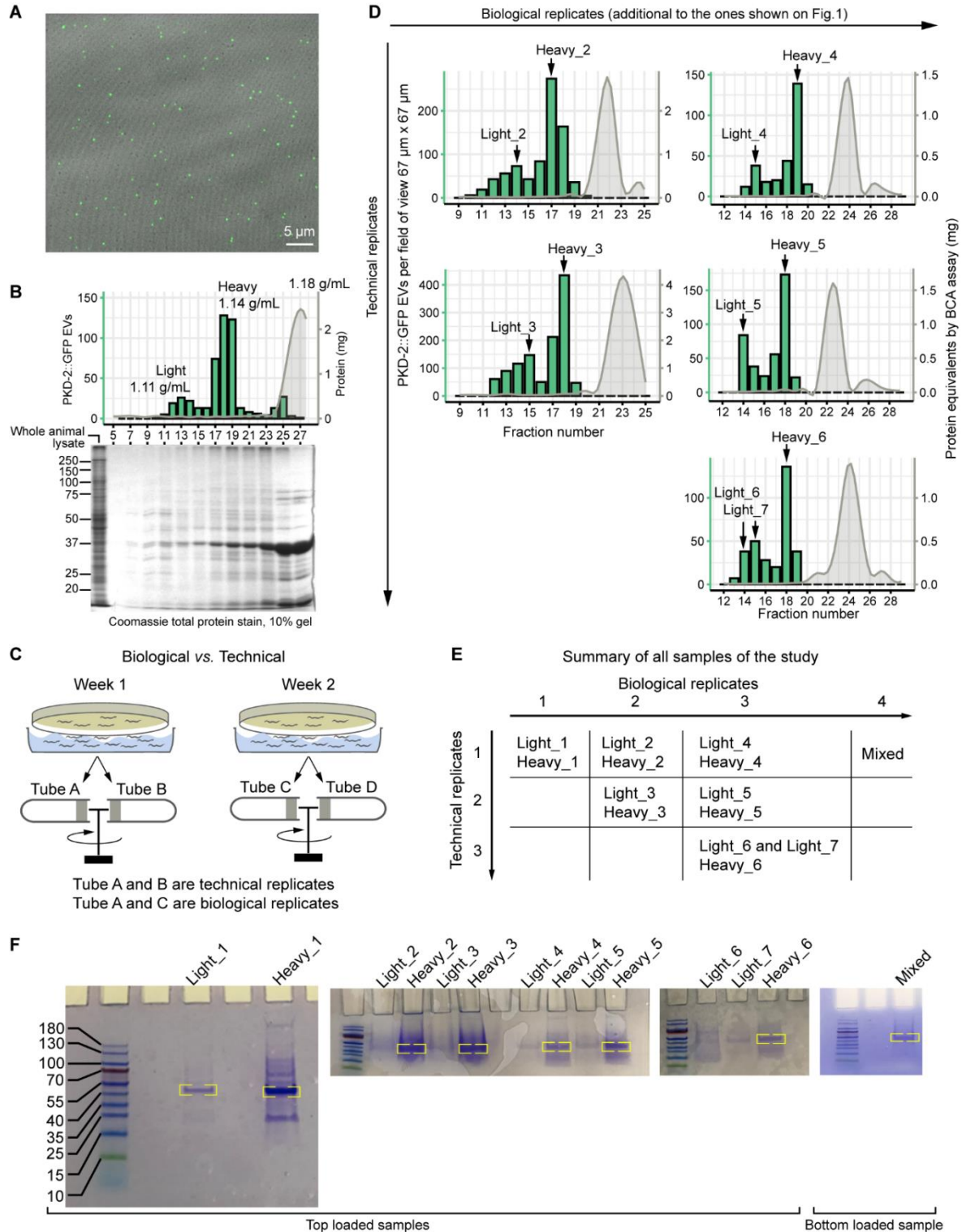
11 Super-resolution imaging was performed on a Zeiss LSM880 confocal system equipped with
12 Airyscan Super-Resolution Detector with Fast Module, 7 Single Photon Lasers (405, 458, 488,
13 514, 561, 594, 633 nm), Motorized X-Y Stage with Z-Piezo, T-PMT. Planes of captured Z-stacks
14 were distanced 0.185 μ m for optimal 3D rendering. Image analysis and processing was
15 performed using Zen Blue 2.0 and Zen Black 2.0.

16 Live imaging of EV release during mating

17 To visualize EV release during mating three *unc-51* hermaphrodites were placed with ten males
18 of the PT3618 strain in the center of an unseeded NGM plate, some bacteria were transferred
19 on the pick to feed the hermaphrodites. The piece of agar with the placed worms (approximately
20 24 x 40 mm) was transferred onto a 24 x 60 coverslip with the worm side facing the coverslip.
21 Then the agar chunk was covered with a 28 x 48 mm saran wrap, with a 10 mm- diameter hole
22 in the center, so that the spot with hermaphrodites was exposed to air through the window. This
23 covering method drove the males toward the center with the hermaphrodites. Mating started
24 within 15 minutes. Imaging was performed using 40x objective.

25
26
27
28

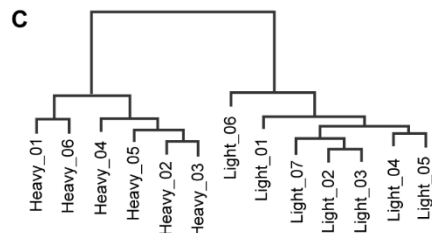
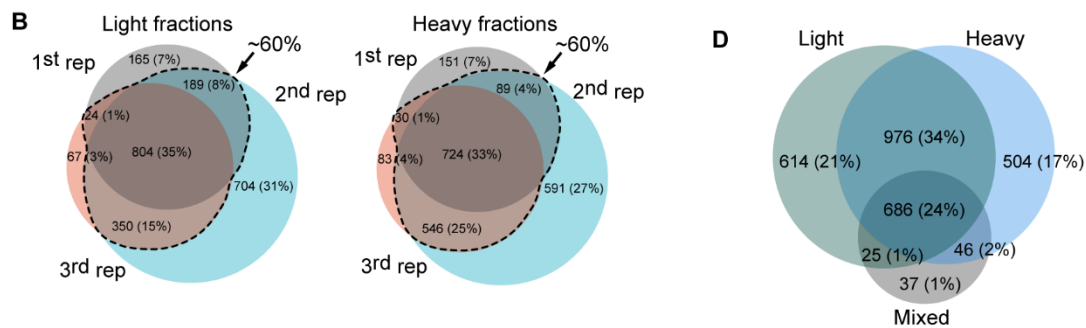
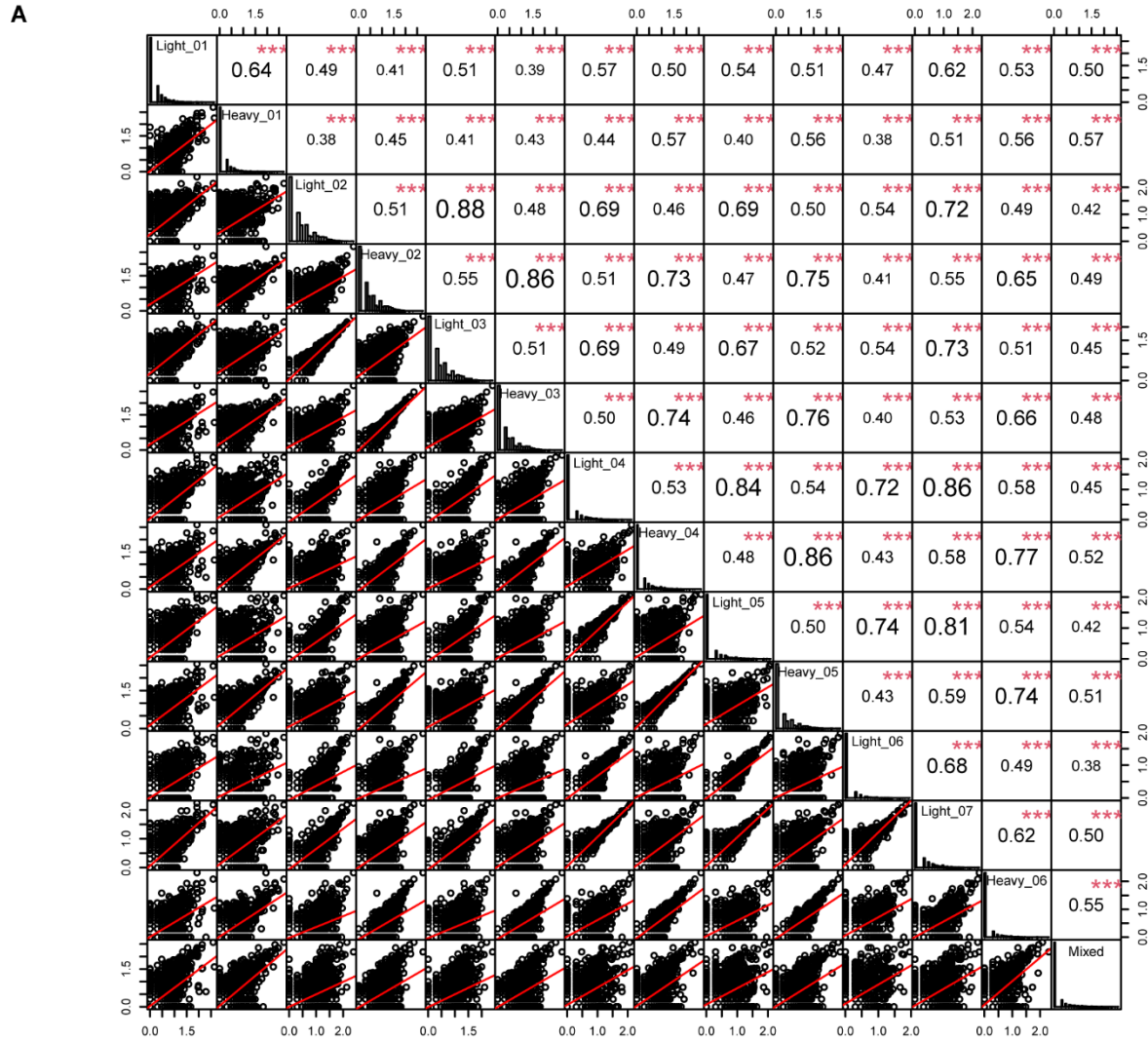
1 **Figure S1.**



2 **Characterization of the EV preparations prior to the mass spectrometry analysis. (A)**
 3 Representative image of the PKD-2::GFP enriched fraction acquired using Zeiss LSM880
 4 microscope and the Airyscan detection system. **(B)** Analysis of protein content across fractions
 5 collected from the isosmotic gradients after buoyant density centrifugation of the crude mixture
 6 of the *C. elegans* and *E. coli* EVs. Combination graph shows a profile of the analyzed EV
 7 preparation. Image of the Coomassie stained gel shows more complex protein composition of
 8

1 the PKD-2::GFP enriched fractions as compared to the fraction of 1.18 g/mL density enriched in
2 most protein. Approximately 40 µg of protein was loaded into each well. **(C)** Biological replicates
3 are represented by EVs harvested on different weeks, technical replicates are represented by
4 EVs that were collected in one prep but equilibrated for their density in different gradients and
5 fractionated into different tubes. **(D)** Fraction profiles of EV preparations for 2 biological
6 replicates (additional to the ones depicted of Figure 1C), each with 2 and 3 technical replicates,
7 respectively. Labeling indicates names of PKD-2 EV enriched fractions that were further
8 analyzed by mass spectrometry. **(E)** Summary of technical and biological replicates of the study.
9 **(F)** Images of stained gels prior to mass spectrometry analysis. Yellow brackets indicate bands
10 that likely represent bacterial outer membrane proteins, and thus were excised from the gel and
11 were not included into protein identification analysis. This approach enriched the remaining
12 proteins further for the EV cargo of *C. elegans*.
13

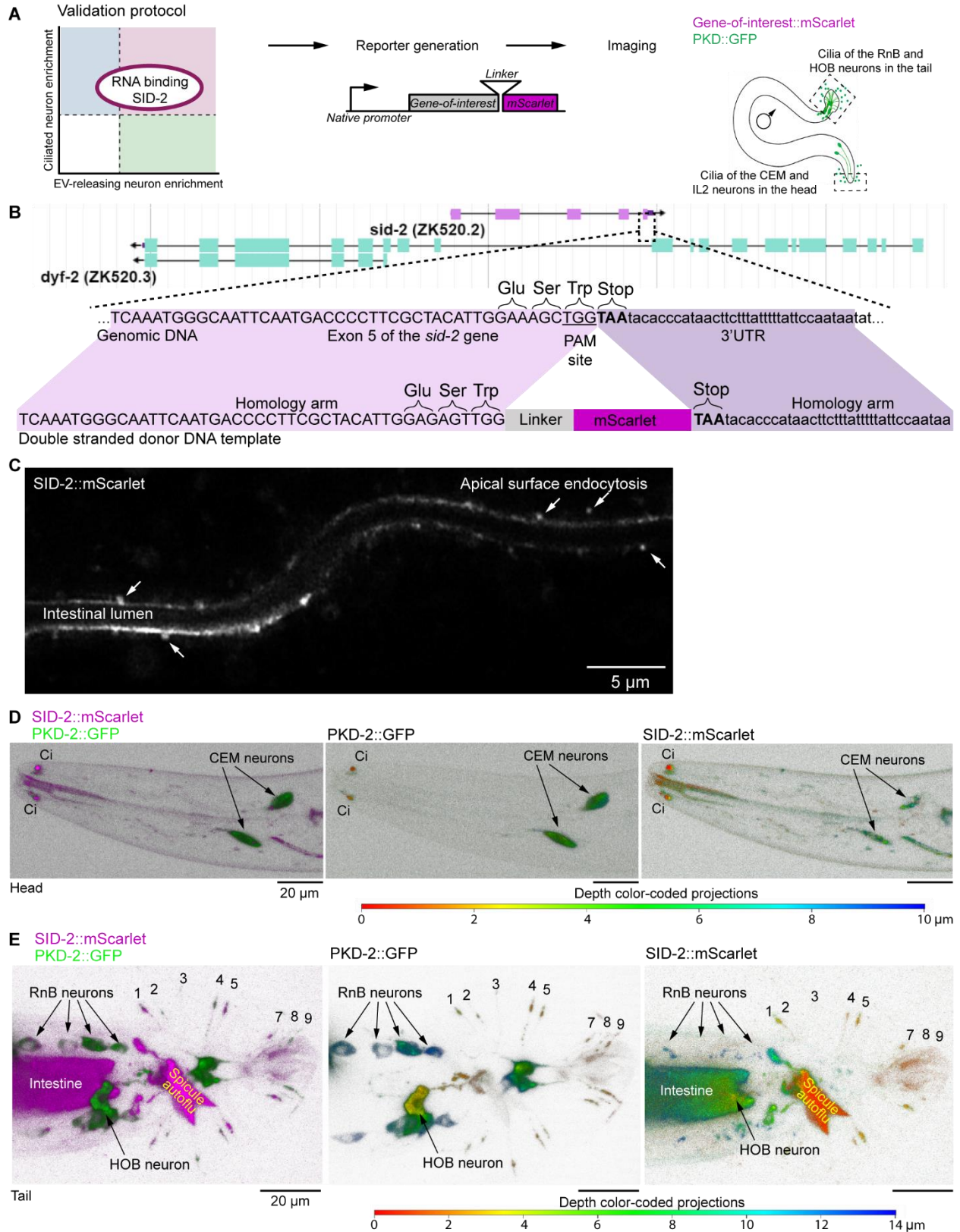
1 **Figure S2.**



3 **Comparison of the identified protein datasets across technical and biological replicates**
 4 **showed high reproducibility of the EV preparation. (A) Sample pairwise comparisons were**

1 made using Spearman correlation analysis. Scatter plots at the bottom left corner compare
2 $\log_{10}(\text{Peptide count}+1)$ values in pairwise manner for all samples of the study; Spearman
3 correlation coefficients for each comparison are at the upper right corner; histograms on the
4 diagonal line show frequencies of $\log_{10}(\text{Peptide count}+1)$ values for each sample [85]. **(B)** Venn
5 diagrams showing overlap in the identified protein datasets of the light and heavy PKD-2::GFP
6 EV subtypes obtained from 3 different biological replicates. **(C)** The cladogram produced by
7 hierarchical clustering of the batch-corrected normalized spectral abundance factors (NSAFs)
8 segregates all the light EV samples from all the heavy ones. **(D)** Light and heavy fractions
9 shared 58% common proteins.

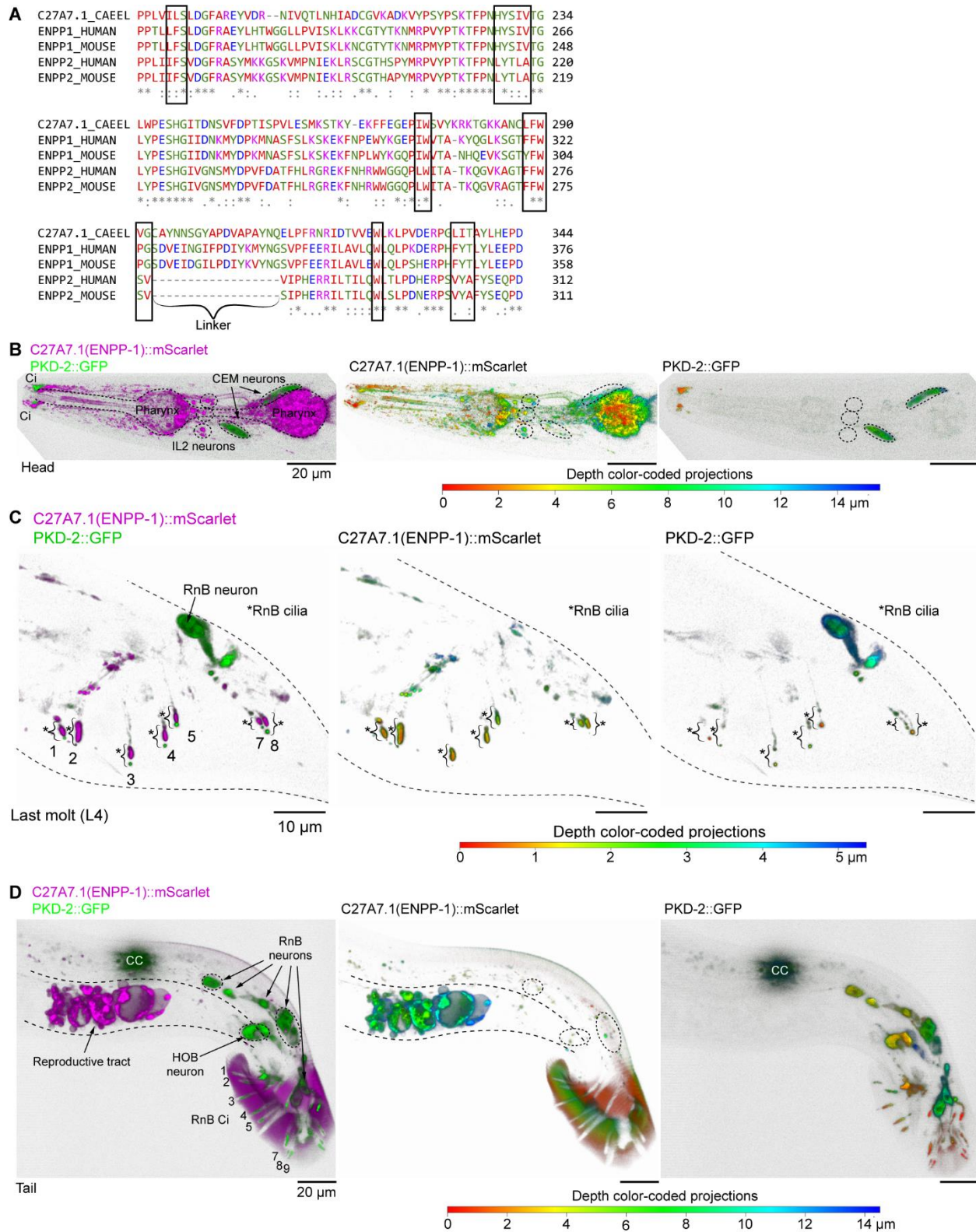
1 **Figure S3.**



2
3

1 **SID-2 nucleic acid binding transmembrane protein is specifically enriched in the male-**
2 **specific ciliated sensory neurons (CEMs, RnBs, and HOB).** (A) Validation protocol for
3 putative ciliary EV cargo. (B) CRISPR/Cas-9-mediated genome editing of the *sid-2* genomic
4 locus. The *sid-2* gene is situated within a long intron of the *dyf-2* gene encoding an ortholog of
5 human ciliary protein WDR19. Editing was performed to generate the SID-2 gene product fused
6 with mScarlet via a 15 amino acid long flexible linker. Two silent mutations were introduced to
7 the protospacer region encoding -Glu-Ser- residues in order to avoid multiple cuts by the Cas9
8 protein. PAM stands for “**p**rotospacer **a**djacent **m**otif” and indicates the targeted site for
9 cleavage by Cas9. (C) Sagittal image through the intestinal lumen showing enrichment of SID-
10 2::mScarlet on the apical surface of the intestinal cells. Ongoing endocytosis of SID-2 is labeled
11 with white arrows. (D-E) 3D projections showing presence of the SID-2::mScarlet reporter in the
12 cilia and cell bodies of the male-specific sensory neurons in the head (D), and in the tail (E).
13 Merged images are shown in 2 colors; individual channels are presented as depth color-coded
14 projections where colocalized presence is indicated by the same color (such as SID-2 and PKD-
15 2 presence within the CEM neurons in (C) is indicated with shades of green and blue which
16 corresponds to ~6 μm distance deep into the acquired Z-stack). Male tail rays housing PKD-2-
17 positive RnB neurons are labeled with numbers. In all male-specific neurons (CEMs, RnBs, and
18 HOB), the SID-2::mScarlet signal was observed in neuronal cell bodies as a few puncta and
19 was mostly accumulated in ciliary regions. SID-2::mScarlet was also observed in two
20 unidentified cells whose processes converge near the hook structure of the male tail.
21

1 **Figure S4.**



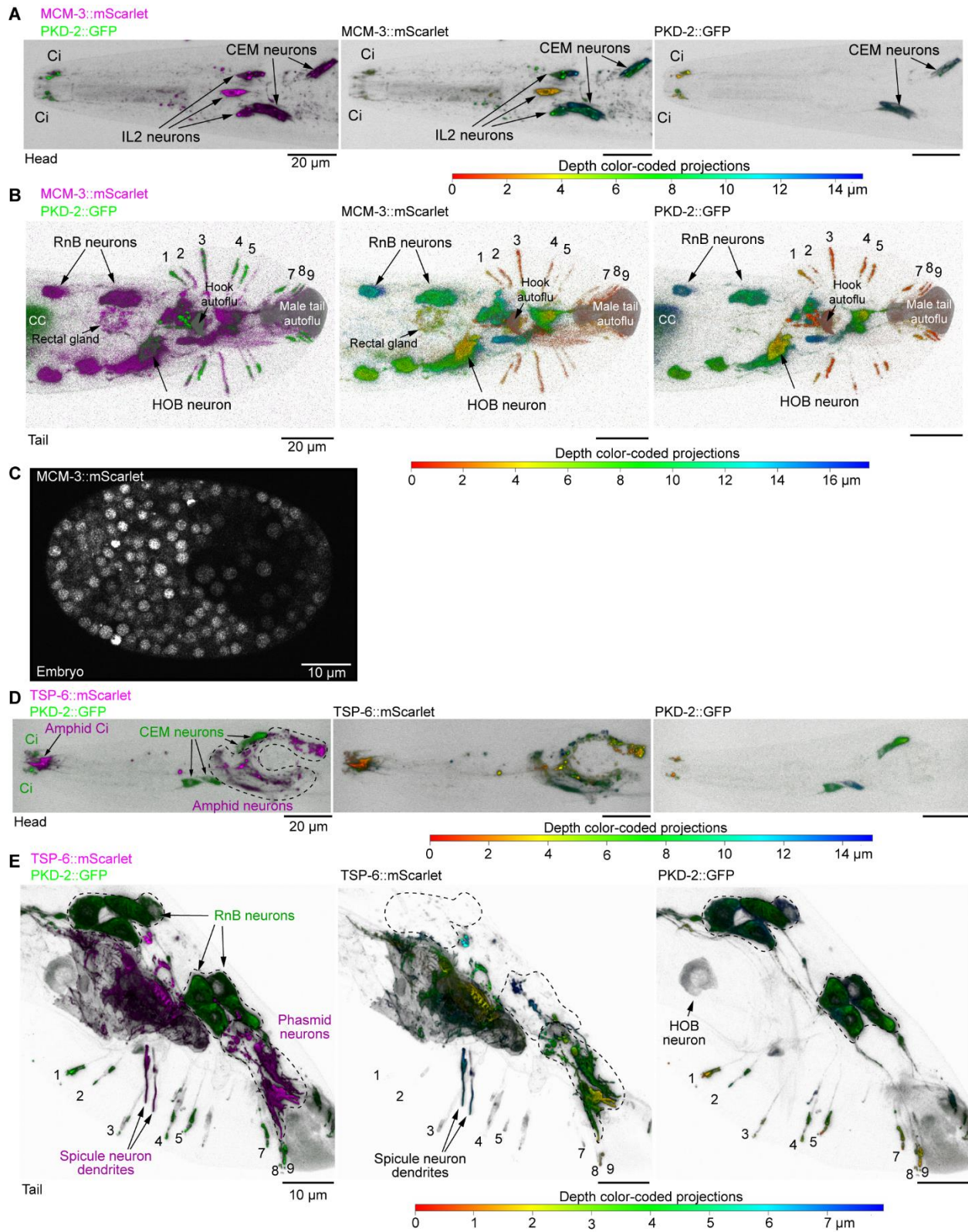
2
3
4
5
6

Ortholog of human ENPP1 (C27A7.1) is specifically expressed in the EV-releasing ciliated sensory neurons (IL2s, CEMs, RnBs, and HOB) and male reproductive tract of *C. elegans*.
(A) Alignment of the phosphodiesterase domain of C27A7.1 to ENPP1 (nucleotide-specific) and

1 ENPP2 (lysophospholipid-specific hydrolase) of human and mouse suggests that C27A7.1 is a
2 nucleotide-specific hydrolase. Black boxes indicate conserved regions forming substrate-binding
3 pockets. Most similarity is observed between C27A7.1 and ENPP1. Figure bracket indicates a
4 linker region of ENPP1 critical for its nucleotide substrate recognition; mutagenic studies show
5 that loss of this linker grants ENPP1 the ability to hydrolase lysophospholipids, yet at much
6 lower efficiency than ENPP2. **(B-D)** 3D projections showing expression pattern of
7 C27A7.1::mScarlet. Merged images are shown in 2 colors; individual channels are presented as
8 depth color-coded projections. C27A7.1 is expressed in pharynx and EV-releasing neurons
9 (EVNs) of the head (CEMs and IL2) (B), and tail (C) as well as in the EVNs of the tail, and the
10 male reproductive tract (D). CC indicates a pair of coelomocytes labeled with GFP as a co-
11 transformation marker of the PKD-2::GFP reporter that remains visible in hermaphrodites.
12 C27A7.1::mScarlet signal also covers the male tail fan indicating that C27A7.1-carrying EVs are
13 adherent to the fan cuticle (D).
14

1 **Figure S5.**

2



3
4

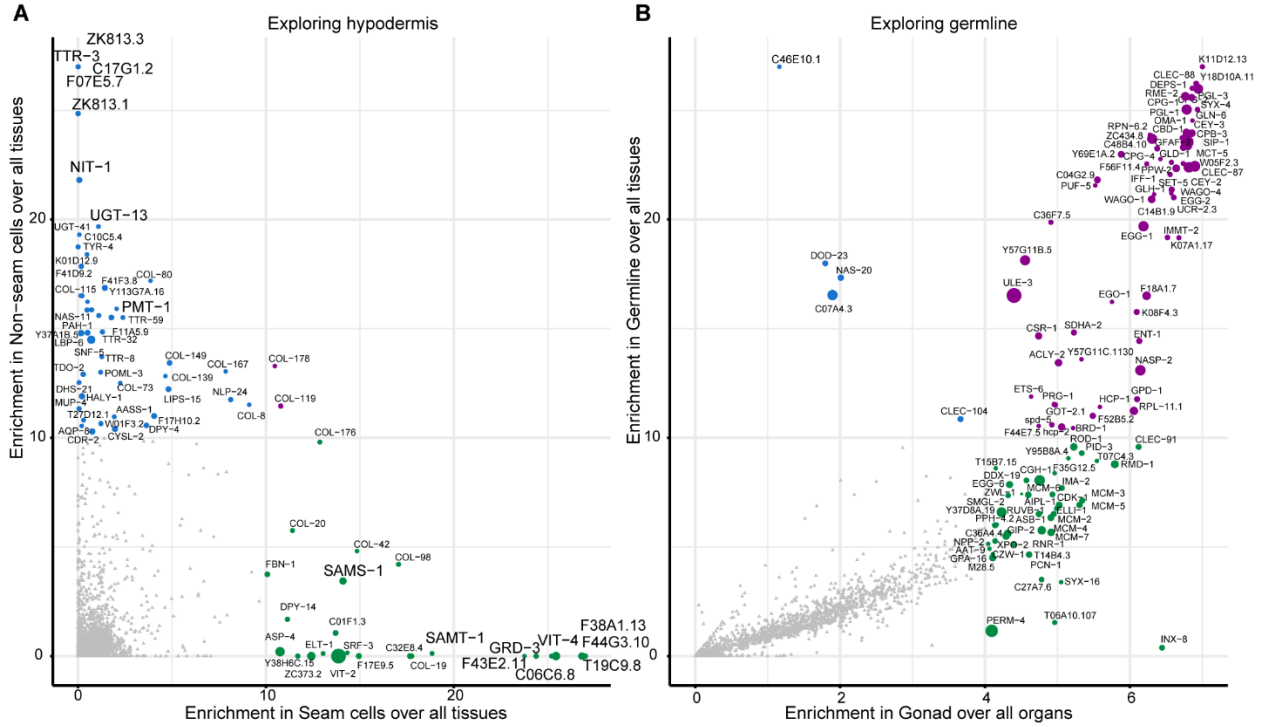
1 **Different neuronal types carry distinct EV cargo; a single neuronal cilium may shed**
2 **multiple cargoes.**

3 **(A-C)** MCM-3 subunit of the replication origin licensing complex is specifically enriched in the
4 EV-releasing ciliated sensory neurons (IL2s, CEMs, RnBs, and HOB). 3D projections showing
5 presence of the MCM-3::mScarlet in the cilia and cell bodies of the EV-releasing sensory
6 neurons in the head – IL2s and CEMs (A), and in the tail – RnBs and HOB (B). Merged images
7 are shown in 2 colors; individual channels are presented as depth color-coded projections.
8 Areas of intense inherent autofluorescence are indicated – the hook structure and the very
9 posterior part of the male tail (B). The MCM-3::mScarlet reporter also shows weak presence in
10 the rectal gland. This identification is based on its similarity to an image in the WormAtlas
11 describing anatomical structures of male proctodeum [86]. **(C)** Sagittal image through the *C.*
12 *elegans* embryo showed nuclear localization of MCM-3::mScarlet in the actively dividing cells.

13 **(D-E)** Ortholog of human CD-9 (TSP-6) is expressed in the amphid and phasmid ciliated
14 neurons, but not in the PKD-2-expressing EV-releasing neurons. 3D projections showing
15 expression pattern of TSP-6::mScarlet at the fourth larval stage. **(D)** Head region, Ci stands for
16 cilia. **(E)** Tail region. TSP-6::mScarlet is expressed in the spicules and other unidentified
17 structures in the mail tail.

18 Merged images are shown in 2 colors; individual channels are presented as depth color-coded
19 projections. PKD-2::GFP served as a marker of the CEM, RnB, and HOB neurons. RnB neurons
20 are labeled with numbers. CC indicates a pair of coelomocytes labeled with GFP as a co-
21 transformation marker. Cilia of the RnB neurons are indicated with numbers.
22

1 **Figure S6.**



2
3
4
5
6

Examples of enrichment plots with tissue-enrichment scores for identified EV cargo candidates. Prediction of EV cargo originating from the hypodermis (A) and germline (B).

1 **Movie S1.**

2 **ENPP-1::mScarlet EV release from the IL2 cilia into the environment.** During the time lapse
3 focus changes from the cilium to EV plane. EVs are connected to each other in a tandem
4 manner and remain attached to the cilium during the course of the video.

5 **Movie S2**

6 **ENPP-1::mScarlet EV release from the male tail during mating to a hermaphrodite.** The
7 footage shows two males mating with one hermaphrodite. Male #1 releases ENPP-1::mScarlet
8 EVs while backing along the body of the hermaphrodite scanning for vulva, whereas Male #2
9 releases ENPP-1::mScarlet EVs during sperm transfer.

10 **Data S1. (separate .xls file)**

11 **Lists of identified peptides and proteins.** (A) Metadata on the overall numbers of peptides
12 and identified proteins from *C. elegans* and *E. coli*. (B) Unique peptides with matched proteins.
13 (C) Non-unique peptides matched with corresponding protein sets. (D) Summary of spectral
14 counts of unique proteins for each gene product. Functions of the genes and human orthologs
15 are indicated. (E) Normalized NSAF values for each identified gene product.

16 **Data S2. (separate .xls file)**

17 **Differential abundance and enrichment analyses.** (A-D) Differential abundance analyses of
18 the light and heavy EV proteomes together with KEGG pathway and InterPro protein domain
19 enrichment analyses. (E) List of ESCRT proteins identified in the EV proteome. (F) List of
20 nucleic acid binding proteins identified in the EV proteome.
21

22 **Data S3. (separate .xls file)**

23 **Mining of the EV proteome.** (A) Overlap of the EVome with the EVN-specific transcriptomes
24 used to produce Figure 2C. (B) IL2 identification table contains relative enrichment values for
25 cholinergic clusters from Cao et al. (2017). (C) EV cargo scores based on their absolute
26 enrichment in ciliated sensory neurons and relative enrichment in the IL2 neurons of
27 hermaphroditic L2 populations; these scores were used to generate the plot on Figure 2F. (D)
28 Overlap of the identified EV proteome with the male-specific transcriptome from [54].
29
30
31
32
33